Chemical Science

ROYAL SOCIETY OF CHEMISTRY

EDGE ARTICLE

View Article Online
View Journal | View Issue

Cite this: *Chem. Sci.*, 2023, **14**, 12098

All publication charges for this article have been paid for by the Royal Society of Chemistry

Structure-guided optimisation of *N*-hydroxythiazole-derived inhibitors of factor inhibiting hypoxia-inducible factor-α†

Thomas P. Corner, [a] Ryan Z. R. Teo, [a] Yue Wu,[b] Eidarus Salah,[a] Yu Nakashima, [c] Giorgia Fiorini,[a] Anthony Tumber,[a] Amelia Brasnett,[a] James P. Holt-Martyn,[a] William D. Figg, Jr.,[a] Xiaojin Zhang, *[b] Lennart Brewitz *[a] and Christopher J. Schofield *[a]

The human 2-oxoglutarate (2OG)- and Fe(II)-dependent oxygenases factor inhibiting hypoxia-inducible factor-α (FIH) and HIF-α prolyl residue hydroxylases 1–3 (PHD1–3) regulate the response to hypoxia in humans *via* catalysing hydroxylation of the α-subunits of the hypoxia-inducible factors (HIFs). Small-molecule PHD inhibitors are used for anaemia treatment; by contrast, few selective inhibitors of FIH have been reported, despite their potential to regulate the hypoxic response, either alone or in combination with PHD inhibition. We report molecular, biophysical, and cellular evidence that the *N*-hydroxythiazole scaffold, reported to inhibit PHD2, is a useful broad spectrum 2OG oxygenase inhibitor scaffold, the inhibition potential of which can be tuned to achieve selective FIH inhibition. Structure-guided optimisation resulted in the discovery of *N*-hydroxythiazole derivatives that manifest substantially improved selectivity for FIH inhibition over PHD2 and other 2OG oxygenases, including Jumonji-C domain-containing protein 5 (~25-fold), aspartate/asparagine-β-hydroxylase (>100-fold) and histone N^{ε}-lysine demethylase 4A (>300-fold). The optimised *N*-hydroxythiazole-based FIH inhibitors modulate the expression of FIH-dependent HIF target genes and, consistent with reports that FIH regulates cellular metabolism, suppressed lipid accumulation in adipocytes. Crystallographic studies reveal that the *N*-hydroxythiazole derivatives compete with both 2OG and the substrate for binding to the FIH active site. Derivatisation of the *N*-hydroxythiazole scaffold has the potential to afford selective inhibitors for 2OG oxygenases other than FIH.

Received 14th August 2023
Accepted 12th October 2023

DOI: 10.1039/d3sc04253g

rsc.li/chemical-science

Introduction

In order to maintain an adequate supply of dioxygen (O_2) to tissues and cells, animals have evolved mechanisms to sense and respond to limiting O_2 availability (hypoxia).[1–3] One such mechanism involves the hypoxia-inducible factor (HIF) system, which regulates genes that work to ameliorate the effects of hypoxia and restore normal O_2 supply.[4–6] HIF is an α/β-heterodimeric transcription factor that plays important roles in both normal physiology and diseases, including cancer, in particular renal cell carcinoma.[7,8] The abundance and transcriptional activity of HIF are controlled in an O_2-dependent manner through post-translational modifications of HIF-α isoforms that are catalysed by the Fe(II)- and 2-oxoglutarate (2OG)-dependent oxygenases prolyl residue hydroxylase domain-containing proteins 1–3 (PHD1–3) and factor inhibiting hypoxia-inducible factor-α (FIH) (Fig. 1A–C).[5,6]

PHD1–3 catalyse the C4-hydroxylation of two prolyl residues (Pro402 and Pro564 in human HIF-1α) in the N- and C-terminal oxygen-dependent degradation domains (ODDs) of HIF-α isoforms (Fig. 1A).[9] The von Hippel-Lindau (pVHL) E3 ubiquitin ligase complex recognizes HIF-α prolyl hydroxylation, leading to polyubiquitination of HIF-α and its proteasomal degradation.[10–12] PHD inhibitors increase HIF-α isoform levels and are used for the treatment of anaemia in chronic kidney disease.[13] By contrast with the PHDs, FIH, which is part of a different structural subfamily of 2OG oxygenases,[14] catalyses the C3-hydroxylation of a HIF-α asparagine residue (Gln803 in human HIF-1α) within the C-terminal activation domains (C-TADs) of HIF-1α and HIF-2α (Fig. 1B).[14,15] HIF-α asparagine residue hydroxylation inhibits the interaction between the HIF-

[a]*Chemistry Research Laboratory, Department of Chemistry and the Ineos Oxford Institute for Antimicrobial Research, University of Oxford, 12 Mansfield Road, OX1 3TA, Oxford, United Kingdom. E-mail: lennart.brewitz@chem.ox.ac.uk; christopher.schofield@chem.ox.ac.uk*

[b]*State Key Laboratory of Natural Medicines, Jiangsu Key Laboratory of Drug Design and Optimization and Department of Chemistry, China Pharmaceutical University, Nanjing 211198, China. E-mail: zxj@cpu.edu.cn*

[c]*Institute of Natural Medicine, University of Toyama, 2630-Sugitani, 930-0194, Toyama, Japan*

† Electronic supplementary information (ESI) available. See DOI: https://doi.org/10.1039/d3sc04253g

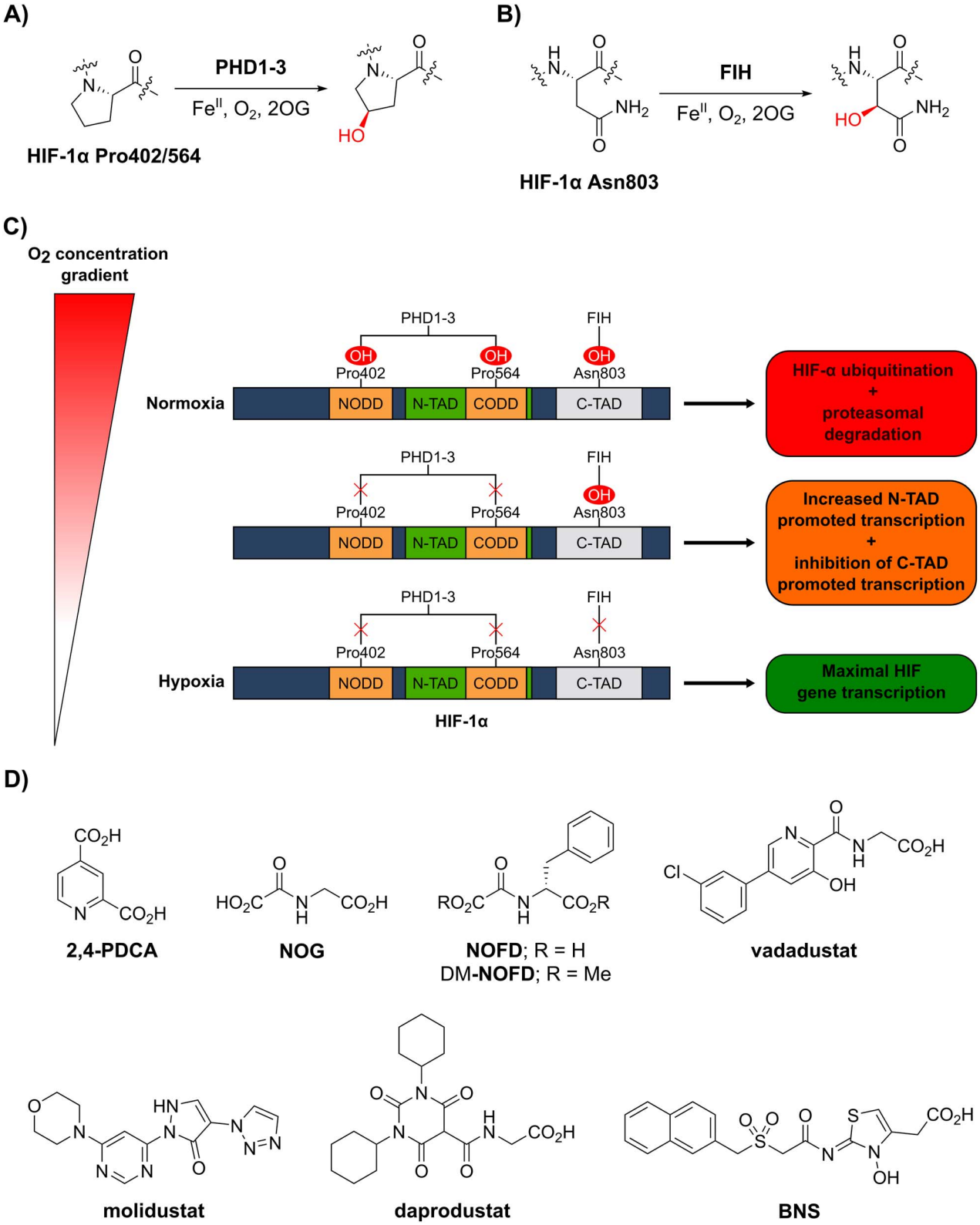

Fig. 1 The human 2-oxoglutarate and Fe(II)-dependent oxygenases PHD1–3 and FIH regulate the transcriptional activity of hypoxia-inducible factor (HIF) isoforms in an O_2 availability-dependent manner by catalysing hydroxylation of HIF-α residues. (A) PHD1–3 catalyse the C4-prolyl-residue hydroxylation of HIF-α (Pro402 and Pro564 in HIF-1α), a modification that promotes HIF-α degradation *via* the ubiquitin-proteasome pathway.[9–12] (B) FIH catalyses the C3-asparaginyl-residue hydroxylation of HIF-α (Asn803 in HIF-1α) resulting in context-dependent suppression of HIF C-terminal activation domain (C-TAD) transcription activity.[14–17] (C) Schematic representation of the role of the PHDs and FIH in the HIF O_2/hypoxia sensing system. (D) Reported FIH inhibitors: the broad-spectrum 2OG oxygenase inhibitors pyridine-2,4-dicarboxylic acid[27] (**2,4-PDCA**) and *N*-oxalylglycine[28] (**NOG**), the FIH-selective inhibitor *N*-oxalyl-D-phenylalanine (**NOFD**)[29] and its dimethyl ester prodrug form dimethyl *N*-oxalyl-D-phenylalanine (DM-**NOFD**). Reported PHD2 inhibitors: vadadustat,[30] molidustat,[31] daprodustat[32] and **BNS**.[17,33]

α C-TADs and the histone acetyl transferases and transcriptional coactivators p300/CBP resulting in suppression of C-TAD-mediated promotion of the transcriptional activity of α,β-HIF.[16,17]

O_2 is a cosubstrate of both PHD1–3 and FIH, with the PHDs being more sensitive to O_2 availability than FIH, as evidenced by kinetic analyses (PHD $K_m(O_2) = 230$–250 μM;[18] FIH $K_m(O_2) = 90$ μM[19]).[20–22] As O_2 levels are depleted, PHD activity decreases, resulting in increased levels of HIF-α. In combination with HIF-β, HIF-α promotes the cellular hypoxic response by increasing the context-dependent expression of genes, including those encoding for erythropoietin (EPO)[23] and vascular endothelial growth factor (VEGF).[24] Under severe hypoxia,[25] the activities of both the PHDs and FIH in cells are inhibited, and C-TAD-mediated promotion of HIF-α,β transcription is increased (Fig. 1C).[1,4,6,26]

Cellular studies have provided evidence that the sets of α,β-HIF target genes that are upregulated in hypoxia vary dependent on the context, including the cell type used.[17,34,35] Exploiting the context-dependent nature of α,β-HIF gene expression is important from a therapeutic perspective, *e.g.* if anaemia treatment *via* α,β-HIF-mediated upregulation of the *EPO* gene is being targeted, concomitant upregulation of VEGF may be undesirable, as the latter has the potential to promote cancer.[36] Interestingly, studies comparing the effects of hypoxia with those of broad spectrum 2OG oxygenase inhibitors or (at least) partially selective PHD inhibitors indicate that broad-spectrum inhibitors might better mimic hypoxia, at least in cells under laboratory conditions.[17]

Factors other than FIH, including other 2OG oxygenase related mechanisms, clearly have potential to regulate α,β-HIF target gene expression, *e.g.* the 2OG dependent JmjC histone N^{ε}-lysine demethylase 4A (KDM4A) is reported to regulate HIF-1α abundance.[37] The modulation of FIH activity is, however, of special interest with respect to controlling the set of α,β-HIF target genes upregulated, because, like the PHDs, it directly modifies HIF-α isoforms.[14,15] There is good evidence that the role of FIH in the HIF system is context dependent.[17] Thus, there is potential for the use of combinations of PHD and FIH inhibitors to 'tune' the set of HIF target genes upregulated, or, preferably, to have a single compound that manifests PHD and FIH inhibition activity, in a manner achieving the desired upregulation of a specific set of α,β-HIF target genes.

The rational control of FIH activity in a manner that leads to predicted physiological outcomes is, however, challenging, in part because of the general complexity of eukaryotic transcriptional regulation and the dynamic O_2 availability-dependent nature of HIF-α levels. Further, by contrast with PHD1–3, for which substrates other than HIF-α have not yet been fully validated,[38] there is biochemical and cellular evidence that FIH catalyses the C3-asparaginyl hydroxylation of multiple non-HIF substrates, including ankyrin repeat domain (ARD)-containing proteins NF-κB,[39,40] apoptosis-stimulating p53-binding protein 2 (ASPP2)[41,42] and Notch.[43] FIH is also reported to catalyse the C3 hydroxylation of residues other than asparagine, including histidine-,[44] tryptophan-[45,46] and aspartate-residues.[47]

Cellular studies employing genetic methods have found that FIH also regulates small-molecule metabolism in addition to its role within the HIF system,[48] potentially reflecting its apparent promiscuity with respect to protein substrates. Interestingly, deletion of the FIH gene in mice results in stimulation of both oxidative metabolism and glycolysis, resulting in an increase in cellular energy consumption.[48] Furthermore, cellular peroxide inhibits hydroxylation of multiple FIH substrates at relatively low concentrations (<0.5 μM), suggesting that FIH may function as a sensor of oxidative stress.[49] The underlying molecular mechanism of how FIH affects small-molecule metabolism and the pathophysiological relevance of the apparent pleiotropic cellular functions of FIH remain unclear. Selective small-molecule FIH inhibitors will therefore be of use to inform on the physiological functions of FIH.[50]

Whilst extensive work has focused on the development of PHD2 inhibitors,[51] resulting *e.g.* in the clinical approval of daprodustat,[32] vadadustat[30] and FG-4592 (roxadustat),[52] few small-molecule FIH inhibitors have been reported (Fig. 1D), and none have been approved for therapeutic use.[53] The broad-spectrum 2OG oxygenase inhibitors pyridine-2,4-dicarboxylic acid (**2,4-PDCA**, FIH IC_{50}: 5.0 μM)[54] and *N*-oxalylglycine (**NOG**, FIH IC_{50}: 0.36 μM), which are structural mimetics of 2OG, inhibit FIH *via* competitive displacement of 2OG at the active site.[27,28] In addition, the reported PHD2 inhibitors vadadustat,[30] molidustat,[31] daprodustat[32] and IOX4[55] inhibit isolated recombinant FIH with weak/moderate potency (IC_{50}s: 29 μM, 66 μM, 21 μM and 31 μM, respectively).[56]

A derivative of **NOG** has been identified with improved selectivity for FIH inhibition, *i.e.* *N*-oxalyl-D-phenylalanine (**NOFD**; FIH IC_{50}: 0.24 μM).[29] **NOFD** manifests excellent selectivity for FIH inhibition over PHD2, and its dimethyl ester prodrug (DM-**NOFD**) has been used to inhibit FIH-catalysed HIF-1α Asn803 hydroxylation in cells.[17,57] However, due to the limited options to chemically modify **NOFD** for further potency and selectivity optimization, and evidence that *N*-oxalyl amino acid derivatives can inhibit other 2OG oxygenases, including aspartate/asparagine-β-hydroxylase (AspH)[58] and the JmjC KDMs,[59] alternative lead scaffolds for FIH inhibitor development, suitable for fine tuning with respect to FIH and PHD inhibition, are required.

Here, we report mass spectrometric and crystallographic evidence that the reported *N*-hydroxythiazole-based PHD inhibitor **BNS**[17,33] (Fig. 1D) is a broad-spectrum inhibitor of 2OG oxygenases, including FIH. Structure-guided SAR studies on the *N*-hydroxythiazole scaffold resulted in the discovery of potent *N*-hydroxythiazole-based small-molecule FIH inhibitors with similar potency to **NOFD**.[29] Mass spectrometry (MS)-based inhibition assays reveal the potential of the *N*-hydroxythiazole scaffold to achieve high levels of selectivity with respect to inhibiting PHD2, and other 2OG oxygenases, *i.e.* Jumoni-C domain-containing protein 5 (JMJD5), AspH and KDM4A. Crystallographic studies inform on the mechanism of FIH inhibition and on the mode of metal binding at the active site. In cell-based studies, optimised *N*-hydroxythiazole-derived FIH inhibitors were found to upregulate the expression of the FIH-dependent HIF target gene *EGLN3* and to reduce adipocyte

lipid accumulation, an observation which supports a proposed role of FIH in metabolic regulation.[48] Importantly, our results imply that modifying the *N*-hydroxythiazole scaffold has potential for the design of selective inhibitors of 2OG oxygenases other than FIH.

Results and discussion

BNS is a broad-spectrum 2OG oxygenase inhibitor and a suitable lead scaffold for FIH-targeted inhibitor development

Considering that the PHD-selective inhibitors vadadustat[30] and molidustat[31] and daprodustat[32] have been shown to moderately inhibit FIH *in vitro*,[56] we initially investigated the effect of other reported PHD2 inhibitors on isolated recombinant human FIH (ESI Table S1†). IC_{50} values were determined using a solid-phase extraction coupled to mass spectrometry (SPE-MS)-based FIH inhibition assay, which monitors the mass change (*i.e.* +16 Da) associated with the FIH-catalysed hydroxylation of a HIF-1α-derived peptide, *i.e.* HIF-1$\alpha_{788–822}$.[60,61] We observed that the reported PHD2 inhibitor **BNS**[17,33] (Fig. 1D) inhibits FIH with similar potency (IC_{50} = 0.30 μM; Table 1, entry iii) as the FIH inhibitor **NOFD** (IC_{50} = 0.24 μM; Table 1, entry iv).[29]

Most reported 2OG oxygenase inhibitors, including the above mentioned PHD inhibitors, coordinate to the active site Fe(II) and compete with 2OG for binding, as pioneered in studies on inhibition of collagen prolyl hydroxylase and plant 2OG oxygenases.[62,63] However, it is unclear how **BNS** binds to the active site of the PHDs; pioneering modelling and kinetic studies with *N*-hydroxythiazole-derived PHD inhibitors suggested two possible 2OG-competitive PHD2 binding modes.[33,64] In each of these, the terminal carboxylate of **BNS** was proposed to bind in a similar manner to the 2OG C5 carboxylate, *i.e.* forming hydrogen bonds with the side chains of Tyr329 and Arg383. The mode of Fe(II) coordination was less clear, with two potential bidentate binding modes being considered – one involving coordination *via* the *N*-hydroxyl group and the exocyclic nitrogen atom of the *N*-hydroxythiazole unit (*i.e.* a 5-membered chelate ring) and the other *via* the *N*-hydroxyl group and the acetamide oxygen atom (*i.e.* a 7-membered chelate ring; Fig. 2A).

To investigate its binding mode to the active site of a 2OG oxygenase, **BNS** was co-crystallised with FIH in the presence of Zn(II), which was used as a catalytically inert surrogate for Fe(II). The structure was solved by molecular replacement (MR) using a reported FIH structure (PDB ID: 4B7K[65]) as a search model. The FIH:Zn:**BNS** complex structure (PDB ID: 8K71; space group: $P4_12_12$, resolution: 2.23 Å) reveals that **BNS** binds at the active site and coordinates Zn(II) in a bidentate manner *via* the *N*-hydroxyl group (O–Zn distance: 2.1 Å) and the *exo*-nitrogen atom (N–Zn distance: 2.7 Å) of its *N*-hydroxythiazole unit (Fig. 2B). Thus, the structural analysis implies that **BNS** binds to FIH *via* the proposed metal binding mode 1 (Fig. 2A); note, that **BNS** might bind to the PHDs *via* different modes; however, our efforts to crystallize **BNS** with PHD2 were unsuccessful.

Superimposition of the FIH:Zn:**BNS** complex structure with reported FIH:Fe:2OG (PDB ID: 1MZF;[66] Cα RMSD = 0.30 Å) FIH:Fe:2OG:HIF-1$\alpha_{786–826}$ (PDB ID: 1H2L;[28] Cα RMSD = 0.28 Å) complex structures indicates that **BNS** competes with both 2OG and HIF-1α for binding FIH (Fig. 2C and D). Notably, the orientation of the metal coordination mode of **BNS** is different to that observed crystallographically for 2OG (Fig. 2C) and **NOFD** (PDB ID: 1YCI;[29] Fig. 2E), as previously observed in FIH structures in complex with daprodustat (PDB ID: 5OP6;[56] Fig. 2F), molidustat (PDB ID: 5OP8;[56] Fig. 2G) and vadadustat (PDB ID: 5OPC;[56] ESI Fig. S5†).[56,67] The hydroxyl group of **BNS** binds Zn(II) in the same manner as the 2OG ketone carbonyl (*i.e.* *trans* to Asp201); however, the interaction between Zn(II) and the *N*-hydroxythiazole *exo*-nitrogen, which occupies the coordination site *trans* to His279, is perpendicular to that observed for the C1 carboxylate of 2OG, which binds *trans* to His199. The carboxylate of **BNS** is positioned to interact with the side chains of FIH residues Tyr145 (2.2 Å), Thr196 (3.0 Å), and Lys214 (2.5 Å), mimicking the interactions of the 2OG C5 carboxylate with FIH (Fig. 2C). In complex with FIH, daprodustat has also been found to engage in hydrogen bonding with Tyr145, Thr196 and Lys214 through its carboxylate group (Fig. 2F).[56] By contrast, in the FIH:Zn:vadadustat complex structure, the carboxylate of vadadustat orients away from the side chains of Tyr145 and Thr196, and only interacts with Lys214 (ESI Fig. S5†).[56] The triazole ring of molidustat is observed crystallographically to

Table 1 Comparison of 2OG oxygenase inhibition by **BNS** with the reported broad-spectrum 2OG oxygenase inhibitors pyridine-2,4-dicarboxylic acid (**2,4-PDCA**) and *N*-oxalylglycine (**NOG**), and the FIH selective inhibitor *N*-oxalyl-D-phenylalanine (**NOFD**)

		IC_{50} [μM][a]				
Entry	Cmpd	FIH[b]	PHD2[c]	AspH[d]	KDM4A[e]	JMJD5[f]
i	**2,4-PDCA**	5.0 ± 2.1 (ref. 54)	5.3 ± 3.4 (ref. 54)	0.03 ± 0.01 (ref. 54)	0.10 ± 0.00	0.33 ± 0.07 (ref. 70)
ii	**NOG**	0.36 ± 0.03	12.3 ± 4.4	1.1 ± 0.3 (ref. 58)	22.1 ± 1.1	0.15 ± 0.02 (ref. 70)
iii	**BNS**	0.30 ± 0.07	0.11 ± 0.00	3.4 ± 0.1	67.4 ± 39.8	0.25 ± 0.01
iv	**NOFD**	0.24 ± 0.02	>100	15.5 ± 1.2 (ref. 60)	14.1 ± 0.0	>100 (ref. 70)

[a] Mean average ± standard deviation (SD) of two independent experiments (each composed of technical duplicates). [b] Using 0.15 μM FIH, 10.0 μM 2OG and 5.0 μM of a HIF-1α C-terminal transactivation domain fragment (HIF-1α C-TAD$_{788–822}$).[61] [c] Using 0.15 μM PHD2$_{181–426}$, 10.0 μM 2OG and 5.0 μM of a HIF-1α C-terminal oxygen-dependent degradation domain fragment (HIF-1α CODD$_{556–574}$).[61] [d] Using 0.05 μM His$_6$-AspH$_{315–758}$, 3.0 μM 2OG and 1.0 μM of a cyclic peptide based on human Factor X (hFX-CP$_{101–119}$).[58] [e] Using 0.15 μM KDM4A, 10.0 μM 2OG and 10.0 μM of a variant of histone 3 (H3$_{1–15}$K9me3$_{1–15}$).[69] [f] Using 0.15 μM JMJD5, 2.0 μM 2OG and 2.0 μM of a 40S ribosomal protein S6 fragment (RSP6$_{128–148}$).[70] Inhibition assays were performed using SPE-MS as described in the ESI.

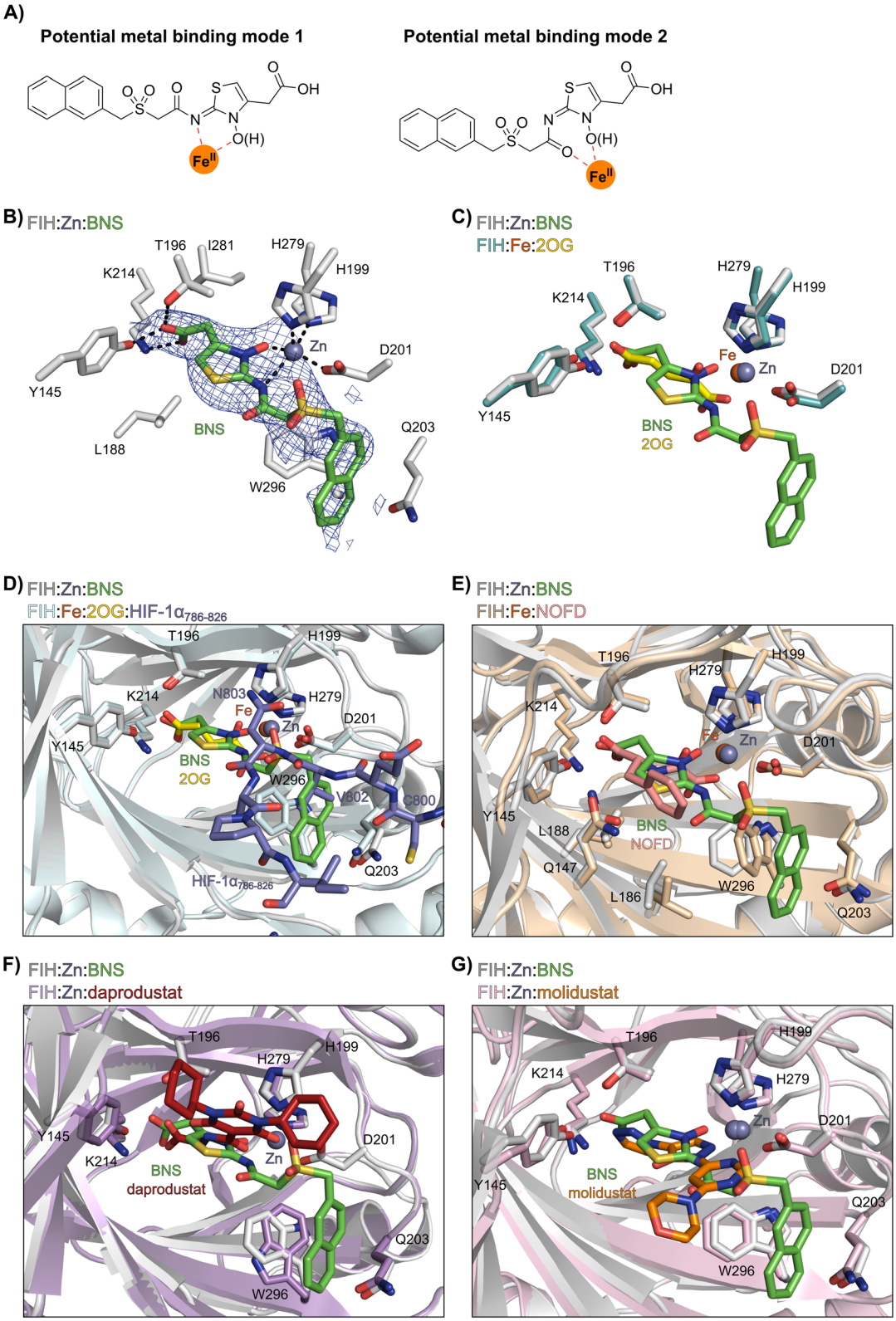

Fig. 2 Crystallographic studies indicate that **BNS** binds to the FIH active site in a 2OG- and HIF-1α-competitive manner. Colour code: light grey: FIH; green: carbon-backbone of **BNS**; yellow: carbon-backbone of 2OG; dark grey: zinc; orange: iron; red: oxygen; blue: nitrogen and yellow: sulphur. (A) Two alternative modes have been proposed for how **BNS** binds to Fe(II) in the PHD2 active site.[33] (B) Active site view from the FIH:Zn:**BNS** complex structure (PDB ID: 8K71) showing the OMIT electron density map (mFo-DFc) contoured to 2.1 σ around **BNS**. (C–F) Superimposition of active site views from the FIH:Zn:**BNS** complex structure and reported (C) FIH:Fe:2OG (PDB ID: 1MZF;[66] teal: FIH), (D) FIH:Fe:2OG:HIF-1$\alpha_{786-826}$ (PDB ID: 1H2L;[28] light blue: FIH; purple: carbon-backbone of HIF-1α), (E) FIH:Fe:**NOFD** (PDB ID: 1YCI;[29] ochre: FIH; pink: carbon-backbone of **NOFD**), (F) FIH:Zn:-daprodustat (PDB ID: 5OP6;[56] light purple: FIH; deep red: carbon-backbone of daprodustat) and (G) FIH:Zn:molidustat (PDB ID: 5OP8;[56] light pink: FIH; orange: carbon-backbone of molidustat) complex structures.

engage in hydrogen bonds with Tyr145 and Lys214; however, not with Thr196 (Fig. 2G).[56]

The FIH structure in complex with **BNS** reveals that the naphthalene group of **BNS** extends into the HIF-1α substrate binding pocket and is positioned to engage in π–π and amide-π stacking interactions with the side chains of Trp296 (face-to-face) and Gln203 (edge-to-face), respectively (Fig. 2D). As a result, the binding of **BNS** to FIH likely disrupts the hydrophobic interaction between the indole group of Trp296 and the conserved hydrophobic substrate residue (*e.g.* Val802 in HIF-1α) that is adjacent to the asparagine residue undergoing hydroxylation, which biochemical studies have shown is essential for efficient FIH catalysis.[68] Analysis of a reported FIH:Zn:2OG:HIF-$1\alpha_{786-826}$ complex structure (PDB ID: 1H2L;[28] Fig. 2D) indicates that the primary amide side chain of Gln203 is involved in substrate recognition, by forming a hydrogen bond with the backbone amide oxygen atom of HIF-1α Cys800. Interestingly, neither daprodustat or molidustat appear to interact with Gln203 and/or Trp296 in complex with FIH (Fig. 2F and G). Given the importance of Gln203 and, in particular, Trp296 for substrate binding,[68] the hydrophobic interactions between the naphthalene unit of **BNS**, Gln203 and Trp296 are potentially contributing factors behind the observed increased in FIH inhibitory activity of **BNS** compared with other PHD inhibitors (>50-fold, as judged by IC_{50} comparison, ESI Table S1†),[56] in addition to the three hydrogen bonds made by the **BNS** carboxylate with FIH, unlike molidustat and vadadustat (ESI Fig. S5†).

To investigate the potential of **BNS** for selective FIH inhibition, its selectivity was investigated with respect to other 2OG-dependent protein oxidising enzymes, that is PHD2, Jumonji-C domain-containing protein 5 (JMJD5), aspartate/asparagine-β-hydroxylase (AspH) and KDM4A, using reported SPE-MS inhibition assays.[58,61,69,70] In addition to PHD2 and KDM4A, we included AspH and JMJD5 in our selectivity studies, because AspH, like FIH, catalyses protein aspartate- and asparagine-residue hydroxylation (although in epidermal growth factor-like domains),[71,72] and because JMJD5 is structurally closely related to FIH.[73,74] The results reveal that, in addition to being a potent PHD2 (IC_{50} = 0.11 μM; Table 1, entry iii) and FIH inhibitor, **BNS** inhibits JMJD5 (IC_{50} = 0.25 μM) and AspH (IC_{50} = 3.36 μM), whereas inhibition of KDM4A was not observed (IC_{50} > 100 μM).

The combined results thus indicate that **BNS** is in fact a relatively broad-spectrum inhibitor of 2OG oxygenases, similar to **2,4-PDCA** and **NOG** (Table 1, entries i and ii). Importantly, however, the results also reveal that the selectivity profile of **BNS** for 2OG oxygenase inhibition differs from that of both **2,4-PDCA** and **NOG**. For example, **2,4-PDCA** inhibits JMJD5, AspH, and KDM4A substantially more efficiently that PHD2 and FIH, whereas **NOG** manifests more potent inhibition of FIH, JMJD5 and AspH than PHD2 and KDM4A. This observation is of interest as it indicates that the use of particular broad-spectrum 2OG oxygenase inhibitors could result in different biological outcomes due to the inhibition of a different subset of 2OG oxygenases.

BNS likely does not inhibit KDM4A because of the different geometry of the KDM4A active site compared to those of FIH, PHD2, JMJD5 and AspH.[75] Thus, superimposition of the FIH:Zn:**BNS** complex structure and a reported KDM4A:Ni:2OG complex structure (PDB ID: 6H8P[76]) indicates that the naphthalene group of **BNS** likely clashes with KDM4A residues Thr289 and Asn290, which form part of β-strand VIII of the rigid β-barrel core fold of the KDM4A active site, therefore preventing efficient binding of **BNS** to KDM4A (ESI Fig. S6†). By contrast, modelling studies predict that **BNS** can likely adopt binding modes within the PHD2, JMJD5 and AspH active sites that are analogous to the FIH:Zn:**BNS** complex structure (Fig. 3A–D).

The *N*-hydroxythiazole core of **BNS** is predicted to bind within the 2OG binding pockets of PHD2, AspH and JMJD5 and to coordinate to the metal in a bidentate manner, consistent with the observation that *N*-hydroxythiazoles inhibit recombinant PHD2 *via* a 2OG-competitive mechanism.[64] The **BNS** carboxylate group is predicted to form hydrogen bond interactions with residues that interact with the 2OG C5 carboxylate (Tyr329 and Arg383 in PHD2;[77] Ser668 and Arg735 in AspH;[78] Tyr272, Ser318 and Lys336 in JMJD5;[74] Fig. 3B–D), as observed in the FIH:Zn:**BNS** complex structure, and the naphthalene unit likely extends into the respective peptide substrate binding pockets.

The docking results also indicate that the sulfone moiety of **BNS** will be positioned to form hydrogen bonds with the side chains of active site residues in PHD2, AspH and JMJD5 (Arg322 in PHD2; Lys666, Arg686 and Arg688 in AspH; Gln275 in JMJD5), an observation that contrasts with the FIH:Zn:**BNS** complex structure, in which the oxygen atoms of the sulfone group are solvent exposed. The residues that are predicted to interact with the sulfone of **BNS** in, at least, AspH[78] and PHD2,[79] have been observed by crystallography to be involved in substrate recognition, suggesting that the sulfone of **BNS** may be important to prevent productive substrate binding to AspH and PHD2.

Notably, the **BNS** modelling study implied that the orientation of the naphthalene unit of **BNS** may be different for **BNS** in complex with PHD2, AspH and JMJD5, as compared with that observed in the FIH:Zn:**BNS** complex structure (Fig. 3A–D). The difference in naphthalene binding may be due to the flexibility of the sulfone and methylene units that connect the *N*-hydroxythiazole core and naphthalene ring of **BNS**, and likely contributes to **BNS** being a relatively broad spectrum 2OG oxygenase inhibitor compared to more structurally rigid 2OG-competitive inhibitors such as daprodustat.

Overall, the above described results indicate that the *N*-hydroxythiazole scaffold of **BNS** is attractive for the development of selective FIH inhibitors, because (i) the FIH:Zn:**BNS** complex structure can be used to guide inhibitor design, (ii) the structure of **BNS** is modular and can be chemically modified, (iii) the **BNS** *N*-hydroxythiazole scaffold has potential for fine tuning inhibition of FIH and the PHDs, and (iv) **BNS** is active in cell-based studies.[17,80] We therefore carried out SAR studies directed at optimising the selectivity of **BNS** for FIH inhibition. As part of the SAR study, the four main structural features of **BNS**, *i.e.* the *N*-hydroxythiazole core, the carboxylate group, the

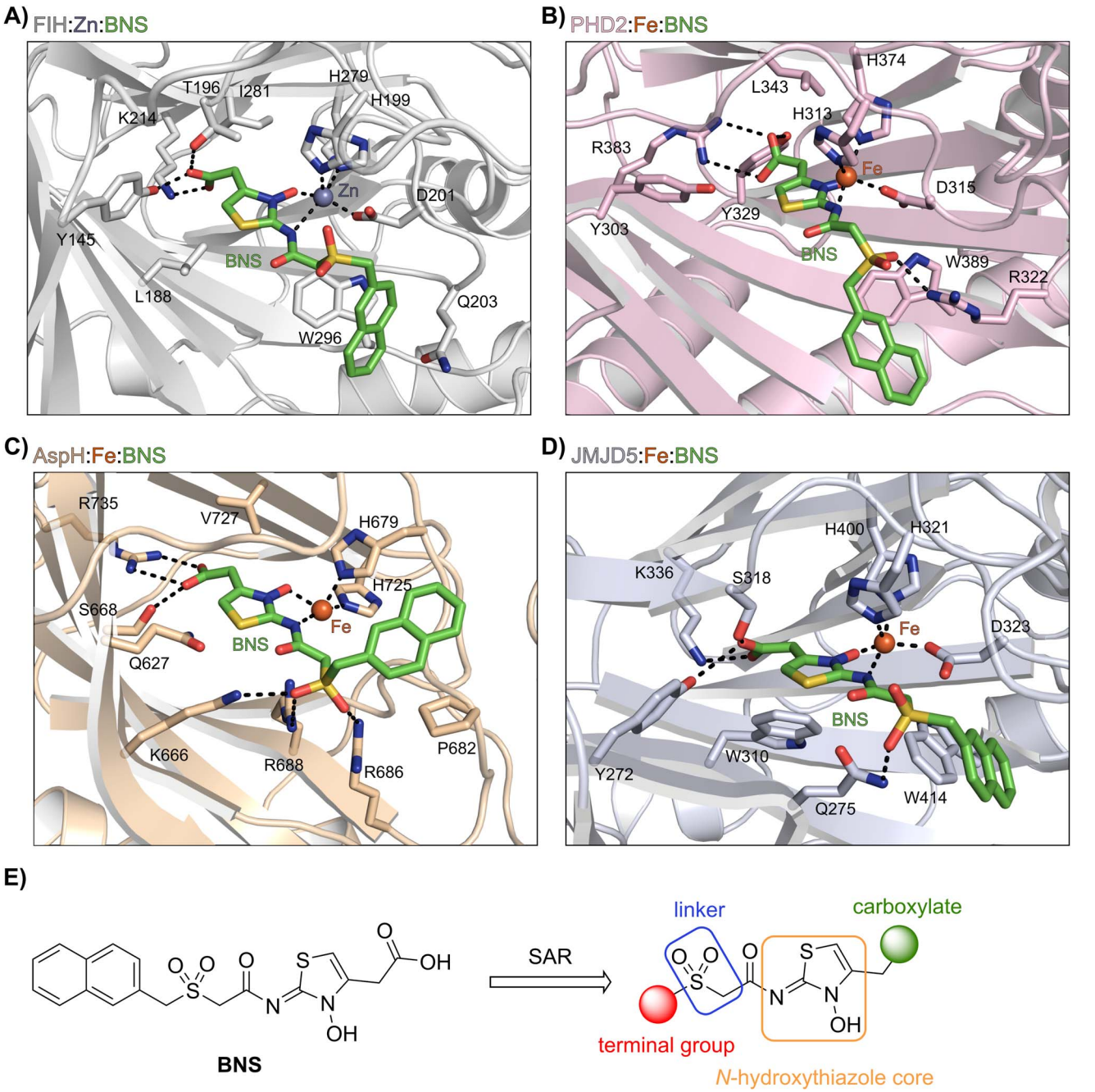

Fig. 3 Docking studies predict that **BNS** may bind to the active sites of PHD2, AspH and JMJD5 with similar binding modes to that observed in the FIH:Zn:**BNS** complex structure. Colour code: green: carbon-backbone of **BNS**; dark grey: zinc; orange: iron; red: oxygen; blue: nitrogen and yellow: sulphur. (A) Active site view from the FIH:Zn:**BNS** complex structure (PDB ID: 8K71; light grey: FIH). (B–D) Active site views from: (B) the PHD2:Fe:**BNS** docking prediction (pink: PHD2), (C) the AspH:Fe:**BNS** docking prediction (ochre: AspH) and (D) the JMJD5:Fe:**BNS** docking prediction (light blue: JMJD5). (E) Outline of the strategies used for selectivity optimisation of the *N*-hydroxythiazole scaffold.

linker region and the terminal naphthalene moiety, were systematically varied (Fig. 3E).

Structure–activity relationship studies towards optimised *N*-hydroxythiazole-based FIH inhibitors

Variations on the *N*-hydroxythiazole core of BNS. To facilitate the planned SAR study, we initially synthesized *N*-hydroxythiazole derivative **4** in which the 2-naphthylmethyl moiety of **BNS** was substituted for a phenyl group, because 2-((phenyl)sulfonyl)acetic acid was commercially available, unlike 2-((2-naphthylmethyl)sulfonyl)acetic acid. *N*-Hydroxythiazole **4** was prepared in three steps from thiazole **1** in an overall yield of 25%, according to a modified literature procedure (Scheme 1).[33,81] Initially, **1** was coupled with 2-(phenylsulfonyl)acetic acid using T3P[82] to generate amide **2**. Subsequent *meta*-chloroperbenzoic acid (mCPBA)-mediated thiazole *N*-oxidation and lithium hydroxide-mediated ester saponification afforded

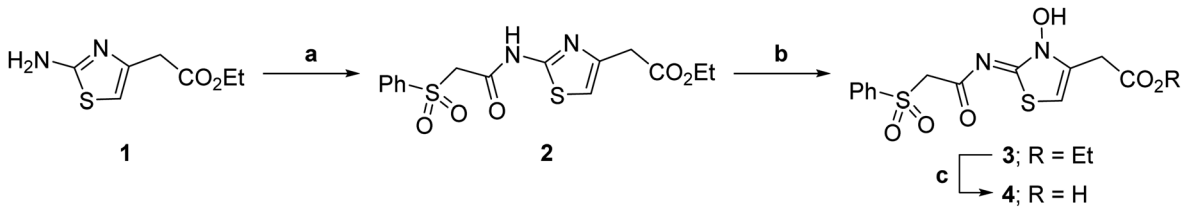

Scheme 1 Synthesis of *N*-hydroxythiazole derivative **4**.[a] [a]Reagents and conditions: (a) 2-(phenylsulfonyl)acetic acid, T3P,[82] *i*Pr$_2$NEt, DMF, 0 °C to rt, 82%; (b) mCPBA, $CHCl_3$, rt, 71%; (c) LiOH, MeOH/H_2O, 0 °C to rt, 43%.

carboxylic acid **4**. Compound **4** and all related *N*-hydroxythiazole derivatives described herein (see below) have been putatively assigned as the (*Z*)-isomers based on a previously reported *N*-hydroxythiazole small-molecule crystal structure[33] and based on the crystal structures of *N*-hydroxythiazole derivatives in complex with FIH reported herein (*e.g.*, Fig. 2B).

Table 2 Inhibition of 2OG human oxygenases by selected thiazole and *N*-hydroxythiazole analogues

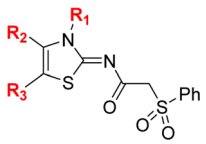

Entry	Cmpd[a]	R_1	R_2	R_3	IC$_{50}$ [μM][b] FIH[c]	PHD2[d]	AspH[e]	KDM4A[f]	JMJD5[g]
i	**BNS**[h]	OH	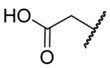	H	0.30 ± 0.07	0.11 ± 0.00	3.4 ± 0.1	67.4 ± 39.8	0.25 ± 0.01
ii	**4**	OH	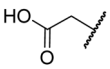	H	0.28 ± 0.00	0.50 ± 0.05	9.6 ± 1.3	>100	0.48 ± 0.01
iii	**5**	H	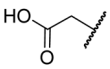	H	>100	>100	>100	>100	>100
iv	**6**	OH	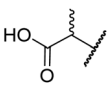	H	61.0 ± 3.1	5.2 ± 2.6	25.6 ± 12.7	>100	60.5 ± 1.0
v	**7**	OH	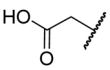	Me	36.7 ± 4.9	3.1 ± 1.4	24.3 ± 12.3	>100	>100
vi	**8**	OH	H	H	>100	>100	>100	>100	>100
vii	**9**	OH	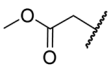	H	>100	>100	96.7 ± 3.2	>100	>100
viii	**3**	OH	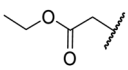	H	>100	>100	68.0 ± 26.8	>100	>100
ix	**10**	OH	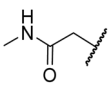	H	>100	>100	43.6 ± 3.7	>100	77.5 ± 23.8
x	**11**	OH	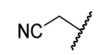	H	>100	>100	>100	>100	>100
xi	**12**	OH	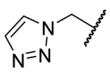	H	>100	>100	83.3 ± 6.7	>100	>100
xii	**13**	OH	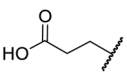	H	2.2 ± 0.6	3.0 ± 1.3	47.3 ± 4.7	>100	>100

[a] All chiral *N*-hydroxythiazole derivatives were prepared as racemic mixtures. [b] Mean average ± SD of two independent experiments (each composed of technical duplicates). [c] Using 0.15 μM FIH, 10.0 μM 2OG and 5.0 μM HIF-1α C-TAD$_{788–822}$.[61] [d] Using 0.15 μM PHD2$_{181–426}$, 10.0 μM 2OG and 5.0 μM HIF-1α CODD$_{556–574}$.[61] [e] Using 0.05 μM His6-AspH$_{315–758}$, 3.0 μM 2OG and 1.0 μM hFX-CP$_{101–119}$.[58] [f] Using 0.15 μM KDM4A, 10.0 μM 2OG and 10.0 μM H3$_{1–15}$K9me3$_{1–15}$.[69] [g] Using 0.15 μM JMJD5, 2.0 μM 2OG and 2.0 μM RSP6$_{128–148}$.[70] [h] **BNS** has a 2-naphthylmethyl sulfonyl group rather than a phenyl sulfonyl group. Inhibition assays were performed using SPE-MS as described in the ESI.

Importantly, the naphthyl to phenyl group substitution of **BNS** did not affect the potency of FIH inhibition; however, it appeared that **4** inhibited PHD2, AspH and JMJD5 less efficiently than **BNS**, thus supporting our proposal that changes in the **BNS** structure can alter its selectivity profile (Table 2, entries i and ii). To investigate the effect of the *N*-hydroxyl group of **4** in FIH inhibition, we synthesized derivative **5** which lacks the *N*-hydroxyl group (ESI Scheme S1†). Notably, **5** did not inhibit the tested 2OG oxygenases (Table 2, entry iii), highlighting the importance of metal chelation for efficient inhibition by *N*-hydroxythiazoles, as indicated by the FIH:Zn:**BNS** complex structure (Fig. 2B).

In the FIH:Zn:**BNS** complex structure, the C5 position of the *N*-hydroxythiazole ring of **BNS** and the methylene unit that connects the *N*-hydroxythiazole ring with the terminal carboxylate are positioned adjacent to the hydrophobic side chains of Leu188 and Ile281, respectively (Fig. 2B). To investigate whether substituents at these positions affect inhibitor potency and selectivity by enhancing hydrophobic interactions with Leu188 and/or Ile281, the corresponding methyl-substituted derivatives of **4** were synthesised, *i.e.* **6** and **7** (ESI Scheme S2†). **6** and **7** showed substantially reduced levels of FIH inhibition compared to **4** (>100-fold; Table 2, entries iv and v), indicating a potential steric clash with the side chains of Leu188 and/or Ile281. Hence, further substitutions at these positions were not explored. Note that, while **7** inhibited PHD2 ~ 30-fold less efficiently than **4**, its selectivity for PHD2 inhibition over FIH inhibition increased by ~20-fold compared to that of **4** (12-fold for **7** *vs.* not PHD2 selective for **4**). **7** also showed no inhibition of JMJD5 and KDM4A (IC_{50} > 100 μM), an observation which may be relevant for the future development of optimised *N*-hydroxythiazole-based PHD2 inhibitors, including with an improved selectivity profile.

Variations on the BNS carboxylate. **BNS** and many other reported 2OG oxygenase inhibitors contain carboxylate groups that mimic binding of the 2OG C5 carboxylate (Fig. 2D).[62] Although **BNS** is active in cells,[17,80] the presence of carboxylates in small-molecule inhibitors can reduce cellular efficacy[83,84] and often requires derivatisation to ester pro-drugs to improve cell-wall permeability.[85] Therefore, 2OG oxygenase inhibitors have been developed in which the carboxylate is replaced with a suitable bioisostere,[31,86,87] which has also been shown to alter the selectivity profile of the inhibitor as different 2OG oxygenases employ different residues to interact with the 2OG C5 carboxylate.[31,62,67,86] Consequently, the *N*-hydroxythiazole analogues **8–12** were prepared (ESI Scheme S3a–e†) to investigate whether removing or replacing the carboxylate group of **BNS** with groups that could engage in similar hydrogen bonding interactions with Tyr145, Thr196 and Lys214, as observed in the FIH:Zn:**BNS** complex structure (Fig. 2B), affects FIH inhibition and selectivity.

The removal of the *N*-hydroxythiazole carboxylate side chain (as in **8**), as well as the substitution of the carboxylate with bioisosteres such as amide (as in **10**), nitrile (as in **11**) and triazole (as in **12**) groups resulted in the complete loss of FIH inhibition (Table 2, entries vi–xi), highlighting the importance of the hydrogen bonding interactions between the carboxylate and the FIH active site residues. Increasing the distance between the carboxylate and *N*-hydroxythiazole ring, as *e.g.* in compound **13** (ESI Scheme S3f†), led to a ~10-fold reduction in both PHD2 and FIH inhibition relative to **4** (FIH IC_{50}: 2.2 μM; Table 2, entry xii). Hence, further modifications of the **BNS** carboxylate group or thiazole C4 substituent were not investigated.

Variations on the BNS methylene sulfone linker. Docking of **BNS** into the PHD2, AspH and JMJD5 active site indicates that its sulfone may interact with the side chains of residues, which, at least for PHD2 and AspH, are involved in substrate binding, *i.e.* Arg322 (PHD2), Lys666, Arg686 and Arg688 (AspH), and Gln275 (JMJD5) (Fig. 3B–D). Since equivalent interactions were not observed in the FIH:Zn:**BNS** complex structure (Fig. 2B), modification of the methylene sulfone linker, which connects the *N*-hydroxythiazole and phenyl groups of **4**, was explored as a potential strategy to enhance selectivity for FIH inhibition. Thus, *N*-hydroxythiazole analogues **14–23** that contain alternative linkers, including amide, sulfonamide, aniline, and ether groups, were prepared *via* modification of the route used for the synthesis of **4**, using alternative carboxylic acid and/or acid chloride coupling partners in the initial amide formation step (ESI Scheme S4†).

Whilst the truncated *N*-acetylated **BNS** derivative **14** was >200-fold less efficient in inhibiting FIH than **4** (IC_{50}: 52.4 μM; Table 3, entry ii), compounds **15–23** were all relatively efficient FIH inhibitors (IC_{50} < 10 μM; Table 3, entries iii–xi). This observation indicates that the terminal phenyl substituent is important for FIH inhibition. Sulfones **4** (IC_{50}: 0.28 μM) and **15** (IC_{50}: 0.30 μM), and sulfonamide **21** (IC_{50}: 0.36 μM) were the most potent FIH inhibitors within this series (Table 3, entries i, iii and ix), an observation which may reflect their increased ability to engage in hydrophobic contacts with the side chains of Gln203 and Trp296, as observed in the FIH:Zn:**BNS** complex structure (Fig. 2B). Both **4** and **21** were also efficient PHD2 inhibitors (IC_{50}s: 0.50 μM and 0.57 μM, respectively). By contrast, **15**, in which an ethylene group connects the *N*-hydroxythiazole core and the sulfone linker, showed decreased inhibition of PHD2 (IC_{50}: 2.7 μM), JMJD5 (IC_{50}: 3.3 μM) and AspH (IC_{50}: 33.0 μM), relative to **4**.

Sulfonamide **20**, which, like sulfone **15**, contains an ethylene chain that bridges the *N*-hydroxythiazole core and sulfonamide linker, and ether **22** also retained potent FIH inhibition (IC_{50}s: 1.0 μM and 0.75 μM, respectively; Table 3, entries viii and x). Furthermore, **20** and **22** did not substantially inhibit KDM4A or AspH, and **20** displayed ~6-fold selectivity for FIH inhibition over PHD2 inhibition and ~13-fold selectivity over JMJD5 inhibition, which is ~3-fold and ~8-fold greater than that of **4**, respectively. This observation indicates that extending the alkylene unit connecting the *N*-hydroxythiazole unit and linker group may be a viable approach to increase selectivity for FIH inhibition, potentially resulting from disruption of the predicted hydrogen bonding interactions by the **BNS** sulfone in the PHD2, JMJD5 and AspH substrate binding sites (Fig. 3B–D). Replacement of the sulfonamide of **20** with an amide (**17**; IC_{50}: 4.6 μM) and truncation of the ethylene chain (**19**; IC_{50}: 3.7 μM)

Table 3 Inhibition of human 2OG oxygenases by selected derivatives of *N*-hydroxythiazole **4** with modifications to the methylene sulfone linker

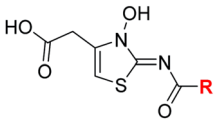

Entry	Cmpd	R	IC_{50} [μM][a] FIH[b]	PHD2[c]	AspH[d]	KDM4A[e]	JMJD5[f]
i	**4**	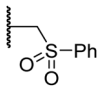	0.28 ± 0.00	0.50 ± 0.05	9.6 ± 1.3	>100	0.48 ± 0.01
ii	**14**	Me	52.4 ± 30.4	>100	>100	>100	3.2 ± 0.7
iii	**15**	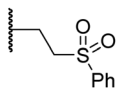	0.30 ± 0.05	2.7 ± 0.2	33.0 ± 12.1	>100	3.3 ± 1.5
iv	**16**	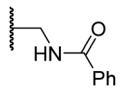	1.2 ± 0.2	1.2 ± 0.2	2.4 ± 1.1	>100	1.7 ± 0.3
v	**17**	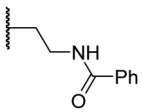	4.6 ± 0.7	3.6 ± 0.4	28.3 ± 6.5	>100	4.6 ± 1.7
vi	**18**	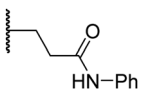	6.0 ± 1.2	2.3 ± 0.1	3.7 ± 1.5	>100	8.4 ± 2.7
vii	**19**	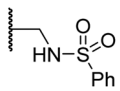	3.7 ± 1.5	15.5 ± 4.6	3.1 ± 0.4	17.4 ± 0.2	12.0 ± 0.6
viii	**20**	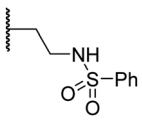	1.0 ± 0.1	6.5 ± 1.8	23.3 ± 10.1	>100	13.4 ± 6.5
ix	**21**	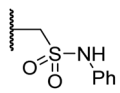	0.36 ± 0.21	0.57 ± 0.18	0.76 ± 0.10	>100	2.8 ± 0.9
x	**22**	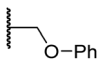	0.75 ± 0.23	2.6 ± 0.2	20.2 ± 6.6	>100	1.2 ± 0.2
xi	**23**	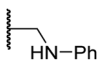	3.2 ± 1.1	10.3 ± 2.9	11.1 ± 0.4	71.6 ± 11.8	4.7 ± 1.1

[a] Mean average ± SD of two independent experiments (each composed of technical duplicates). [b] Using 0.15 μM FIH, 10.0 μM 2OG and 5.0 μM HIF-1α C-TAD$_{788–822}$.[61] [c] Using 0.15 μM PHD2$_{181–426}$ and 5.0 μM HIF-1α CODD$_{556–574}$.[61] [d] Using 0.05 μM His$_6$-AspH$_{315–758}$, 3.0 μM 2OG and 1.0 μM hFX-CP$_{101–119}$. [e] Using 0.15 μM KDM4A, 10.0 μM 2OG and 10.0 μM H3$_{1–15}$K9me3$_{1–15}$.[69] [f] Using 0.15 μM JMJD5, 2.0 μM 2OG and 2.0 μM RSP6$_{128–148}$.[70] Inhibition assays were performed using SPE-MS as described in the ESI.

led to a ~5-fold and ~4-fold loss in FIH inhibition, respectively (Table 3, entries v and vii).

Interestingly, sulfonamide **21** was the most active inhibitor of AspH among the tested *N*-hydroxythiazole derivatives (IC_{50}: 0.76 μM; Table 3, entry ix), being ~5-fold more potent than **4**. Docking studies indicate that the sulfonamide moiety of **21** may be appropriately positioned to interact with the polar side chains of Arg686, Arg688 and Glu617 (ESI Fig. S10†). AspH is a proposed medicinal chemistry target[54,88] associated with the pathologies of various cancers,[89,90] including hepatocellular carcinoma[88,91] and pancreatic cancer,[93] hence, derivatisation of **21** to develop potent AspH inhibitors warrants further investigation.[92]

Linker rigidification improves selectivity for FIH inhibition. The ethylene chain connecting the *N*-hydroxythiazole core and the sulfone/sulfonamide linker groups of compounds **15** and **20** is likely conformationally flexible in solution. As predicted for the naphthalene group of **BNS**, this flexibility may enable the terminal phenyl unit to occupy different conformations within the substrate binding pockets of FIH, PHD, JMJD5 and AspH

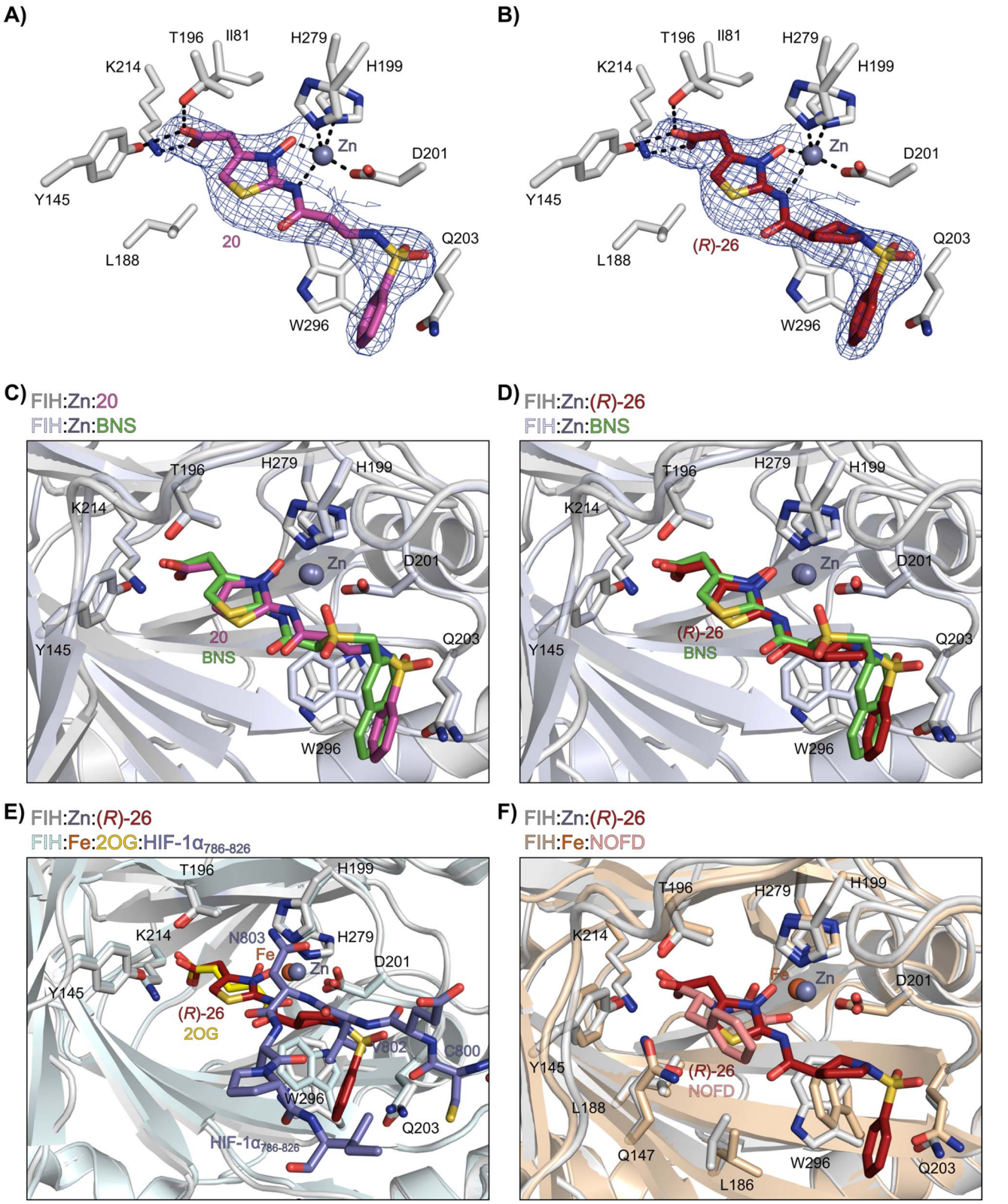

Fig. 4 *N*-Hydroxythiazole derivatives **20** and **26** bind to the FIH active site in a similar manner to **BNS**. Colour code: light grey: FIH; purple: carbon-backbone of **20**; ruby: carbon-backbone of (*R*)-**26**; green: carbon-backbone of **BNS**; dark grey: zinc; orange: iron; red: oxygen; blue: nitrogen and yellow: sulphur. (A) View from the FIH:Zn:**20** complex structure (PDB ID: 8K72) showing the OMIT electron density map (mFo-DFc) contoured to 2.1 σ around **20**. (B) View from the FIH:Zn:**26** complex structure (PDB ID: 8K73) showing the OMIT electron density map (mFo-DFc) contoured to 2.1 σ around **26**. (C) Superimposition of active site views from the FIH:Zn:**20** and the FIH:Zn:**BNS** (PDB ID: 8K71, FIH: light blue) complex structures. (D–F) Superimposition of active site views from the FIH:Zn:**26** complex structure and (D) the FIH:Zn:**BNS** complex structures (PDB ID: 8K71, FIH: light blue), (E) a reported FIH:Fe:2OG:HIF-1$\alpha_{786-826}$ complex structure (PDB ID: 1H2L;[28] light blue: FIH; yellow: carbon-backbone of 2OG; purple: carbon-backbone of HIF-1$\alpha_{786-826}$), and (F) a reported FIH:Fe:**NOFD** complex structure (PDB ID: 1YCI;[29] ochre: FIH; pink: carbon-backbone of **NOFD**).

(Fig. 3), thus potentially limiting selectivity. We therefore investigated whether rigidification of the linker chain *via* cyclisation would increase selectivity for FIH inhibition. Sulfonamide **20** was considered more appropriate to initially test this hypothesis than **15** due to the commercial availability of suitable cyclic β-amino acid derivatives that enable facile modification of **20**. Thus, we co-crystallised FIH with **20** to guide further SAR studies (FIH:Zn:**20**; PDB ID: 8K72; space group: $P4_12_12$, resolution: 2.25 Å).

Analysis of the FIH:Zn:**20** complex structure revealed that **20** adopts an FIH binding pose similar to that of **BNS** (Fig. 4A and C). Notably, the phenyl ring of **20** did not engage in a π-stacking interaction with the side chain of Trp296, as observed for the naphthalene unit of **BNS** in complex with FIH, but instead forms a face-to-face amide-π interaction with the primary amide group of Gln203. The reduced potency of FIH inhibitor **20** compared with **4** and **BNS** (*i.e.* ∼3-fold), may be a result of the lack of interaction with Trp296. Importantly, however, there appeared to be sufficient space adjacent to the ethylene unit of **20** in the FIH:Zn:**20** complex structure to potentially allow for its substitution with a carbocycle, which may also interact productively with the indole side chain of Trp296. Thus, *N*-hydroxythiazole derivatives **24–30**, in which carbocycles substitute for the ethylene chain of **20**, were synthesised to test this proposal (ESI Scheme S5†) and their inhibition of FIH, PHD2, JMJD5, AspH and KDM4A was determined (Table 4).

The use of a β-pyrrolidine linker (**26**; Table 4, entry iv) increased FIH inhibition potency by ∼2-fold relative to **20** (IC_{50}: 0.50 μM) and enhanced selectivity for FIH inhibition over PHD2 (∼25-fold), JMJD5 (∼25-fold) and AspH (∼75-fold) inhibition; **26** did not inhibit KDM4A (IC_{50} > 100 μM). The increased rigidity of the pyrrolidine ring of **26**, compared with the ethylene unit of **20**,

Table 4 Inhibition of human 2OG oxygenases by *N*-hydroxythiazole analogues bearing carbocyclic linkers

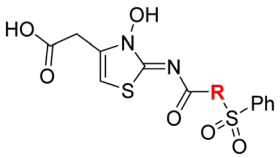

Entry	Cmpd[a]	R	IC_{50} [μM][b] FIH[c]	AspH[d]	PHD2[e]	KDM4A[f]	JMJD5[g]
i	**20**	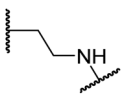	1.0 ± 0.0	23.3 ± 10.1	6.5 ± 1.8	>100	13.4 ± 6.5
ii	**24**	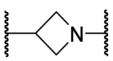	0.45 ± 0.17	60.9 ± 24.1	5.2 ± 0.7	>100	29.1 ± 4.4
iii	**25**	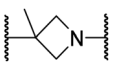	1.2 ± 0.2	>100	33.5 ± 1.0	>100	32.6 ± 6.7
iv	**26**	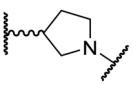	0.50 ± 0.02	37.8 ± 11.3	12.4 ± 0.8	>100	12.5 ± 1.0
v	**27**	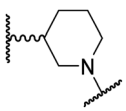	0.87 ± 0.04	49.1 ± 1.7	11.0 ± 1.6	>100	13.4 ± 1.0
vi	**28**		2.1 ± 1.5	24.9 ± 12.0	12.7 ± 1.8	>100	2.6 ± 0.2
vii	**29**	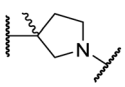	>100	>100	>100	>100	>100
viii	**30**	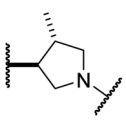	1.7 ± 0.4	>100	71.7 ± 26.6	>100	25.6 ± 0.6

[a] All chiral *N*-hydroxythiazole derivatives were prepared as racemic mixtures. [b] Mean average ± SD of two independent experiments (each composed of technical duplicates). [c] Using 0.15 μM FIH, 10.0 μM 2OG and 5.0 μM HIF-1α C-$TAD_{788–822}$.[61] [d] Using 0.05 μM His_6-$AspH_{315–758}$, 3.0 μM 2OG and 1.0 μM hFX-$CP_{101–119}$.[58] [e] Using 0.15 μM $PHD2_{181–426}$, 10.0 μM 2OG and 5.0 μM HIF-1α $CODD_{556–574}$.[61] [f] Using 0.15 μM KDM4A, 10.0 μM 2OG and 10.0 μM $H3_{1–15}$K9me$3_{1–15}$.[69] [g] Using 0.15 μM JMJD5, 2.0 μM 2OG and 2.0 μM $RSP6_{128–148}$.[70] Inhibition assays were performed using SPE-MS as described in the ESI.

is likely responsible for the increased selectivity of **26**, by limiting the potential binding modes of the terminal phenyl ring. Decreasing the linker ring size from a β-pyrrolidine to an azetidine (**24**; Table 4, entry ii) had no effect on FIH inhibition (IC_{50}: 0.45 μM); however, the selectivity of compound **24** for FIH over PHD2 inhibition (12-fold) was reduced by ∼2-fold compared to **26**. 3-Methylazetidine (**25**; Table 4, entry iii) and β-piperidine (**27**; Table 3, entry v) analogues showed decreased FIH inhibition (IC_{50}s: 1.2 and 0.87 μM, respectively) relative to **26**.

Analysis of a crystal structure of FIH complexed with β-pyrrolidine derivative **26** (FIH:Zn:**26**, PDB ID: 8K73; space group: $P4_12_12$, resolution: 2.25 Å) reveals that **26** binds to the FIH active site in a similar manner to ethylamine derivative **20**, with its phenyl sulfonamide moiety adopting an almost identical conformation for both compounds (Fig. 4A and B), that is engaging in a face-to-face amide-π stacking interaction with the side chain of Gln203. Notably, the β-pyrrolidine ring of **26** is positioned to form hydrophobic interactions with Trp296, as observed with the naphthalene ring of **BNS** (Fig. 2B), which likely contributes to the increased FIH inhibition by **26**, compared with **20**, in addition to the reduced entropic cost of binding. Analysis of the electron density maps for the FIH:Zn:**26** structure indicates that only (*R*)-**26** binds to FIH, despite **26** being present as a racemic mixture, suggesting that the inhibitory activity of the two **26** enantiomers likely differs. Thus, the structural analyses support our proposal that the observed increase in selectivity for FIH inhibition may be a result of stabilising the conformation that binds to the FIH active site.

A substantial decrease in inhibition potency was observed for the α-pyrrolidine analogue of **26** (*i.e.* **28**; IC_{50}: 2.1 μM, Table 4, entry vi), potentially reflecting a steric clash with the FIH active site, in particular with Trp296, and/or loss of the favourable amide-π stacking interaction between the phenyl ring and Gln203, as observed in the FIH:Zn:**26** complex (Fig. 4B), due to the geometry of the α-pyrrolidine ring. These results indicate that a β-pyrrolidine ring, as in **26**, is preferred for achieving both FIH inhibition and selectivity over PHD2, JMJD5, AspH and KDM4A. The addition of a methyl substituent at the C3 position of the β-pyrrolidine ring (**29**; Table 4, entry vii) results in a complete loss of FIH inhibition (IC_{50} > 100 μM), while the *trans*-4-methylpyrrolidine derivative (**30**; Table 4, entry viii) shows decreased levels of FIH inhibition (IC_{50}: 1.7 μM), but improved selectivity for FIH inhibition over PHD2 and AspH relative to **26**.

Variations on the terminal sulfonamide substituent. Having identified compound **26** as a potent FIH inhibitor that displays >25-fold selectivity with respect to PHD2, JMJD5, AspH and KDM4A inhibition, structurally related *N*-hydroxythiazoles **33**-**43** were prepared to investigate the effect of modifying the terminal phenyl group on FIH inhibitor potency (Scheme 2).

The introduction of a chlorine substituent at the *ortho*- (**33**; IC_{50}: 0.39 μM), *meta*- (**34**; IC_{50}: 0.44 μM) or *para*-position (**35**; IC_{50}: 0.46 μM) of the phenyl ring of **26** had negligible effects on inhibitor potency (Table 5, entries ii–iv). Similarly, FIH inhibition was not affected by electron donating (**36**; IC_{50}: 0.46 μM) or electron withdrawing (**37**; IC_{50}: 0.47 μM) substituents at the *para*-position of the phenyl ring (Table 5, entries v and vi), although selectivity over JMJD5 was enhanced ∼5-fold for trifluoromethyl-substituted **37**, relative to **26**. Cyclopentyl derivative **43** manifested reduced levels of FIH inhibition (IC_{50}: 0.81 μM, Table 5; entry xii), which might relate to the loss of the amide-π stacking interaction between the phenyl ring of **26** and Gln203, as observed in the FIH:Zn:**26** complex structure.

The most potent FIH inhibitors identified from this series were biphenyl sulfonamide derivative **38** (IC_{50}: 0.26 μM), ether **39** (IC_{50}: 0.29 μM), and the benzyl derivative **42** (IC_{50}: 0.28 μM) (Table 5; entries vii, viii and xi). These compounds displayed comparable levels of FIH inhibition to the (partially) selective FIH inhibitor **NOFD** (IC_{50}: 0.24 μM) and the broad-spectrum 2OG oxygenase inhibitor **NOG** (IC_{50}: 0.36 μM), and were ∼10-fold more potent than **2,4-PDCA** (IC_{50}: 5.0 μM)[54] (Table 6, entries i–iii). Excellent selectivity for FIH inhibition over AspH and KDM4A inhibition was also observed (>100-fold and >300-fold, respectively); **42** manifested ∼25-fold selectivity for FIH inhibition over PHD2 and JMJD5 inhibition.

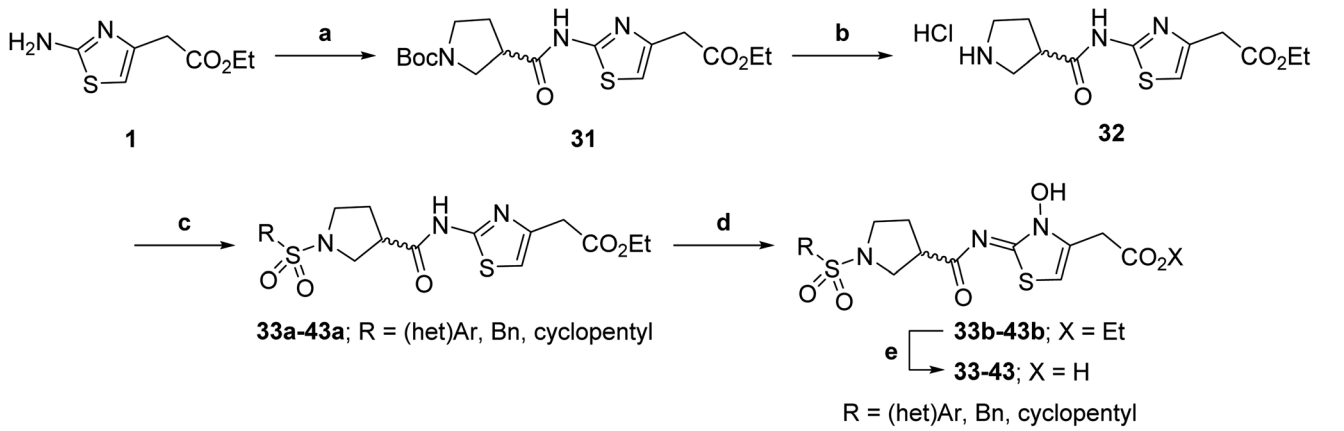

Scheme 2 Synthesis of *N*-hydroxythiazole derivatives **33–43**.[a,b] [a](a) *N*-Boc-pyrrolidine-3-carboxylic acid, T3P,[82] iPr_2NEt, DMF, 0 °C to rt, 99%; (b) HCl/dioxane, 0 °C to rt, 83%; (c) $PhSO_2Cl$, Et_3N, CH_2Cl_2, 0 °C to rt, 78–95%; (d) mCPBA, $CHCl_3$, rt, 24–67%; (e) LiOH, $MeOH/H_2O$, 0 °C to rt, 28–82%. [b]Chemical structures of R groups are shown in Table 5.

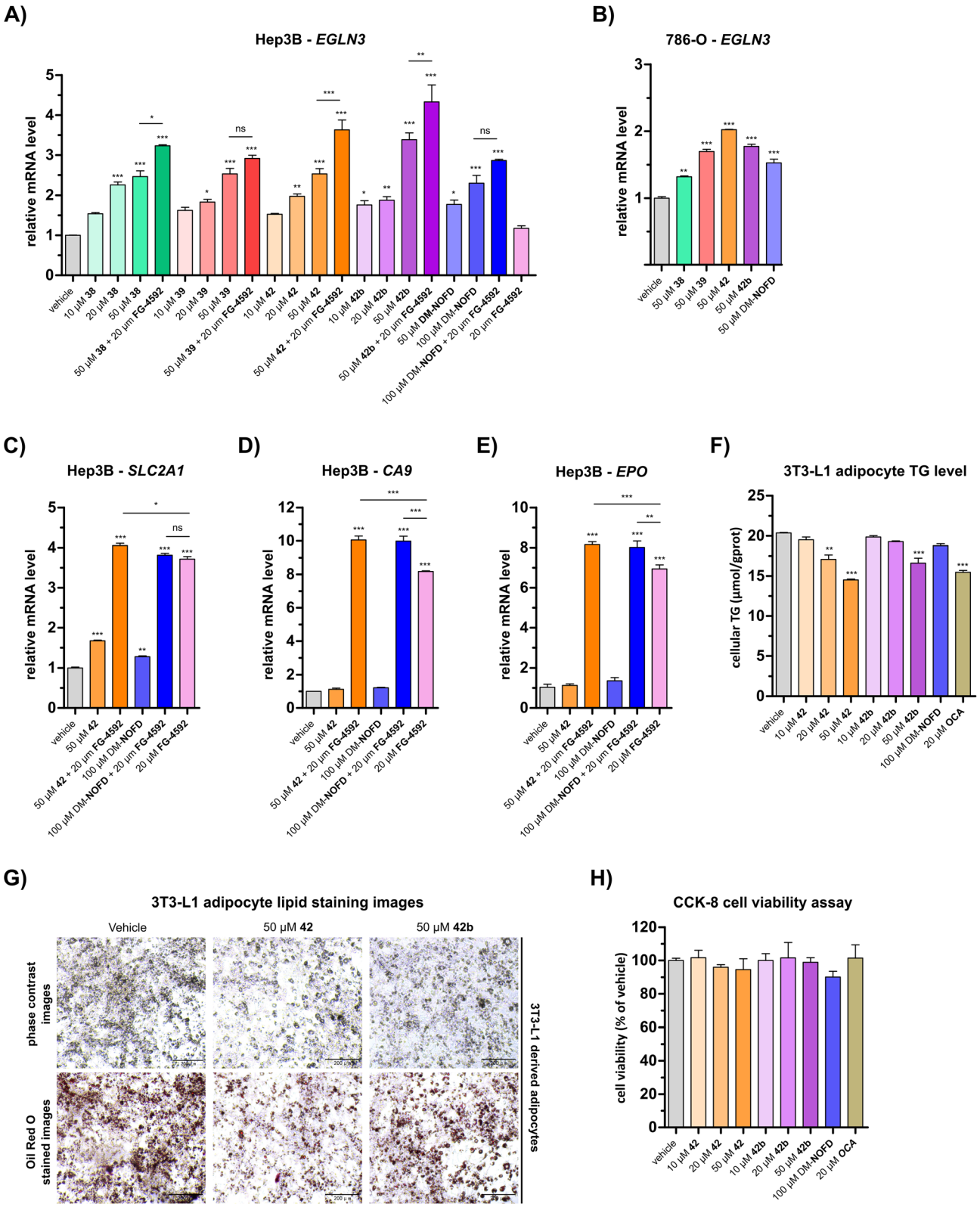

Fig. 5 *N*-Hydroxythiazole-based FIH inhibitors modulate HIF target gene expression in cells and reduce adipocyte lipid accumulation. (A and B) Quantitative Real Time PCR (qRT-PCR) analyses showing the effects of *N*-hydroxythiazole-based FIH inhibitors **38**, **39**, **42** and the ethyl ester prodrug form of **42** (*i.e.* **42b**), dimethyl *N*-oxalyl-D-phenylalanine (DM-**NOFD**) and FG-4592 on prolyl hydroxylase domain-containing protein 3 (*EGLN3*) expression levels in (A) Hep3B and (B) 786-O cells relative to a negative inhibition control (DMSO). (C–E) qRT-PCR analyses showing the effects of **42**, DM-**NOFD**, and FG-4592 on (C) solute carrier family 2 member 1 (*SLC2A1*), (D) carbonic anhydrase 9 (*CA9*) and (E) erythropoietin (EPO) expression levels in Hep3B cells relative to negative inhibition control (DMSO). (F) The cellular triglyceride (TG) levels of 3T3-L1 derived adipocytes following treatment with **42**, **42b**, DM-**NOFD**, the reported farnesoid X receptor (FXR) agonist obeticholic acid (OCA) and a negative inhibition control (DMSO), as

Interestingly, the results indicate that **42** exhibits a different selectivity profile compared to **NOFD** with respect to the other 2OG oxygenases tested. **NOFD** displays greater selectivity for inhibition of FIH over PHD2 and JMJD5 (**NOFD**: >300-fold selective; **42**: ~25-fold selective, as judged by IC_{50} values; Table 6). Whereas, **42** manifests improved selectivity for AspH (**NOFD**: ~65-fold selective; **42**: >100-fold selective) and KDM4A (**NOFD**: ~60-fold selective; **42**: >300-fold selective). The difference in 2OG oxygenase selectivity likely reflects the different binding modes of **NOFD** compared with the *N*-hydroxythiazole-derived FIH inhibitors, as indicated by superimposition of the FIH:Fe:**NOFD** and FIH:Zn:**26** and complex structures (Fig. 4F).

Crystallographic studies have shown that the benzyl side chain of **NOFD**, which occupies a hydrophobic pocket in the FIH active site (formed by Tyr102, Tyr145, Gln147 and Leu186; ESI Fig. S11†), which has not yet been observed in the active sites of some other 2OG oxygenases, including PHD2, is responsible for the selectivity of **NOFD** for FIH inhibition over PHD2. In the reported PHD2:Mn:**NOG** complex structure (PDB ID: 5L9R),[79] the pro-*R* methylene hydrogen atom of **NOG** is orientated towards the side chain of Leu343, which would likely clash with the benzyl substituent of **NOFD**, so preventing efficient binding of **NOFD** to PHD2. By contrast, we propose that the FIH selectivity of **26** and **42** arises, at least in part, due to the rigidity of the β-pyrrolidine ring and the formation of productive interactions with the side chains of residues involved in FIH substrate recognition, *i.e.* Gln203 and Trp296.

Cellular studies

***N*-Hydroxythiazole-based FIH inhibitors modulate cellular expression of FIH-dependent HIF target genes.** At least in some cells, the FIH-catalysed asparagine residue hydroxylation in the C-TAD of HIF-α isoforms inhibits the interaction between HIF-α and the histone acetyl transferases/transcriptional coactivators p300 and CBP, thus resulting in context-dependent suppression of C-TAD-mediated promotion of HIF target gene expression.[17] The prolyl hydroxylase domain-containing protein 3 gene (*EGLN3*) is a HIF target gene, which is apparently negatively regulated by FIH catalysis, potentially in a context-dependent manner.[17,56] We therefore investigated the effect of the *N*-hydroxythiazole-based FIH selective inhibitors **38**, **39** and **42** (Table 5), as well as the corresponding ethyl ester analogue of **42** (*i.e.* **42b**), on *EGLN3* expression levels using DM-**NOFD**[17] as a positive FIH inhibition control.

Quantitative real time PCR (qRT-PCR) analyses revealed a dose-dependent increase in *EGLN3* mRNA levels following the treatment of human hepatocyte carcinoma-derived Hep3B cells with **38**, **39**, **42**, or **42b** (Fig. 5A). At 50 μM, carboxylic acids **38**, **39** and **42** increased *EGLN3* expression by ~2.5-fold relative to the negative inhibition control (*i.e.* DMSO). An apparently greater increase (~3.4-fold) was observed for the ethyl ester **42b** at 50 μM. By comparison, use of 50 μM DM-**NOFD** increased *EGLN3* levels by ~1.8-fold, indicating the *N*-hydroxythiazole derivatives manifest similar, if not greater, cellular efficacy compared to DM-**NOFD** (Fig. 5A). Since they also display weak PHD2 inhibition (Table 6), it cannot be ruled out that **38**, **39**, **42** or **42b** cause weak HIF-α upregulation, that, along with FIH inhibition, contributes to the upregulation of *EGLN3* levels observed in their presence. Note, however, that **NOFD** upregulates *EGLN3* levels and has little, if any, PHD2 inhibition activity (Table 6).

We investigated the effect of **38**, **39**, **42** and **42b** in the presence of the PHD inhibitor FG-4592 (FG-4592, roxadustat),[52] which stimulates an increase in HIF-α levels, to explore whether the effect on *EGLN3* expression would alter. When co-administered with **38**, **42** or **42b**, FG-4592 caused an greater increase in *EGLN3* upregulation relative to the effect of **38**, **42** or **42b** alone (Fig. 5A); FG-4592 alone had no effect on Hep3B *EGLN3* levels. These results support the proposal that FIH catalysis negatively regulates expression of the HIF target gene *EGLN3* through a HIF-dependent mechanism. Interestingly, no additional effect on *EGLN3* levels was observed for FG-4592 with either **39** or DM-**NOFD**, even at 100 μM DM-**NOFD**, compared to use of **39** or DM-**NOFD** alone, an observation requiring further investigation, and one which illustrates the complexity of the biochemistry of HIF transcriptional regulation. We also investigated the effect of the *N*-hydroxythiazole-derived FIH inhibitors **38**, **39**, **42** and **42b**, and DM-**NOFD** on *EGLN3* gene expression in VHL-deficient renal cell carcinoma-derived 786-O cells. Due to the absence of VHL, PHD-mediated HIF degradation does not operate in 786-O cells leading to elevated HIF levels. As with Hep3B cells, we observed upregulation of *EGLN3* with all compounds tested, including DM-**NOFD** (Fig. 5B).

The effect of **42** and DM-**NOFD** on the expression of three additional proposed HIF target genes in Hep3B cells,[17] *i.e.* solute carrier family 2 member 1 (*SLC2A1*; Fig. 5C), carbonic anhydrase 9 (*CA9*; Fig. 5D) and erythropoietin (*EPO*; Fig. 5E), with and without FG-4592, was subsequently investigated by qPCR. *SLC2A1* levels were increased significantly with FG-4592 (~4-fold), and, to a lesser extent with **42** (~1.5-fold) and DM-**NOFD** (~1.3-fold). *EPO* and *CA9* were also strongly upregulated by FG-4592 (~7-fold and ~8-fold, respectively) and showed no response to treatment with either **42** or DM-**NOFD**. By contrast, an increase in *CA9* and, to a lesser extent, *EPO* levels was observed when **42** and DM-**NOFD** were administered in combination with FG-4592, compared with when FG-4592 was used alone. By contrast, no synergistic effect was observed for **42** and DM-**NOFD** in combination with FG-4592 on *SLC2A1* gene expression.

Overall, the cellular results are in agreement with previous work that implying dual inhibition of both FIH and PHDs may be necessary to induce substantial expression of some, but not

determined by a triglyceride colorimetric assay. (G) Representative images of 3T3-L1 derived adipocytes treated with **42** and **42b**, after staining with Oil Red O. Scale bar, 200 μm. (H) The effects of **42**, **42b**, DM-**NOFD** and OCA on 3T3-L1 derived adipocyte cell viability, as measured using the CCK-8 cell viability assay.[95] Values shown are percentages (%) relative to the negative inhibition control (DMSO). Mean average ± SD of three independent experiments are shown. Results were analysed with one-way ANOVA followed by Tukey's multiple comparison test (ns, $p > 0.05$; *, $p < 0.05$; **, $p < 0.01$; ***, $p < 0.001$). Cell-based studies were performed as described in the ESI.†

Table 5 Inhibition of human 2OG oxygenases by *N*-hydroxythiazole analogues bearing different terminal sulfonamide substituents

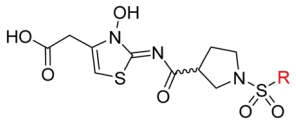

Entry	Cmpd[a]	R	IC_{50} [μM][b] FIH[c]	PHD2[d]	AspH[e]	KDM4A[f]	JMJD5[g]
i	**26**		0.45 ± 0.17	12.4 ± 0.8	37.8 ± 11.3	>100	12.5 ± 1.0
ii	**33**		0.39 ± 0.04	8.0 ± 0.2	30.3 ± 12.6	>100	11.9 ± 1.8
iii	**34**	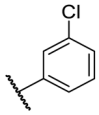	0.44 ± 0.03	14.6 ± 3.2	35.0 ± 0.0	>100	18.5 ± 1.0
iv	**35**	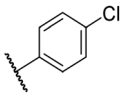	0.46 ± 0.01	9.2 ± 0.4	28.8 ± 8.9	>100	37.7 ± 0.9
v	**36**	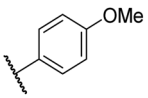	0.46 ± 0.01	9.8 ± 0.5	36.6 ± 2.8	>100	16.0 ± 6.8
vi	**37**	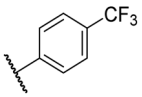	0.47 ± 0.07	15.2 ± 3.6	36.0 ± 0.7	>100	63.2 ± 6.1
vii	**38**	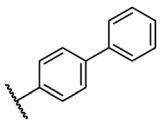	0.26 ± 0.01	3.1 ± 0.1	30.2 ± 10.9	>100	31.9 ± 2.0
viii	**39**	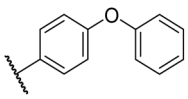	0.29 ± 0.03	3.1 ± 0.2	29.8 ± 4.3	>100	8.6 ± 0.2
ix	**40**	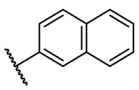	0.45 ± 0.08	5.2 ± 1.1	40.1 ± 2.2	>100	62.8 ± 0.4
x	**41**		0.47 ± 0.07	11.2 ± 2.3	30.3 ± 8.0	>100	15.4 ± 7.1
xi	**42**	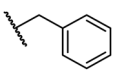	0.28 ± 0.02	6.9 ± 0.5	43.1 ± 18.7	>100	7.2 ± 2.8
xii	**43**		0.81 ± 0.18	9.9 ± 0.5	35.5 ± 3.2	>100	17.4 ± 6.0

[a] All chiral *N*-hydroxythiazole derivatives were prepared as racemic mixtures. [b] Mean average ± SD of two independent experiments (each composed of technical duplicates). [c] Using 0.15 μM FIH, 10.0 μM 2OG and 5.0 μM HIF-1α C-$TAD_{788–822}$.[61] [d] Using 0.15 μM $PHD2_{181–426}$, 10.0 μM 2OG and 5.0 μM HIF-1α $CODD_{556–574}$.[61] [e] Using 0.05 μM His_6-$AspH_{315–758}$, 3.0 μM 2OG and 1.0 μM hFX-$CP_{101–119}$.[58] [f] Using 0.15 μM KDM4A, 10.0 μM 2OG and 10.0 μM $H3_{1–15}K9me3_{1–15}$.[69] [g] Using 0.15 μM JMJD5, 2.0 μM 2OG and 2.0 μM $RSP6_{128–148}$.[70] Inhibition assays were performed using SPE-MS as described in the ESI.

necessarily all, HIF target genes. Note, it cannot be ruled out that other mechanisms, including inhibition of the PHDs or other 2OG oxygenases potentially involved in HIF target gene expression by **42** or DM-**NOFD**, or (*e.g.*) inhibitor mediated effects on the location or the availability of HIF-α isoforms, may contribute towards the observed effects.

Table 6 Comparison of human 2OG oxygenase inhibition by optimised *N*-hydroxythiazole derivatives and **BNS** with the reported FIH inhibitors 2,4-PDCA, NOG and NOFD[29]

		IC_{50} [μM][a]				
Entry	Cmpd	FIH[b]	PHD2[c]	AspH[d]	KDM4A[e]	JMJD5[f]
i	**2,4-PDCA**	5.0 ± 2.1 (ref. 54)	5.3 ± 3.4 (ref. 54)	0.03 ± 0.01 (ref. 54)	0.10 ± 0.00	0.33 ± 0.07 (ref. 70)
ii	**NOG**	0.36 ± 0.03	12.3 ± 4.4	1.1 ± 0.3 (ref. 58)	22.1 ± 1.1	0.15 ± 0.02 (ref. 70)
iii	**NOFD**	0.24 ± 0.02	>100	15.5 ± 1.2 (ref. 60)	14.1 ± 0.0	>100 (ref. 70)
iv	**BNS**	0.30 ± 0.07	0.11 ± 0.00	3.4 ± 0.1	67.4 ± 39.8	0.25 ± 0.01
v	**26**	0.45 ± 0.17	12.4 ± 0.8	37.8 ± 11.3	>100	12.5 ± 1.0
vi	**38**	0.26 ± 0.01	3.1 ± 0.1	30.2 ± 10.9	>100	31.9 ± 2.0
vii	**39**	0.29 ± 0.03	3.1 ± 0.2	29.8 ± 4.3	>100	8.6 ± 0.2
viii	**42**	0.28 ± 0.02	6.9 ± 0.5	43.1 ± 18.7	>100	7.2 ± 2.8

[a] Mean average ± SD of two independent experiments (each composed of technical duplicates). [b] Using 0.15 μM FIH, 10.0 μM 2OG and 5.0 μM HIF-1α C-$TAD_{788–822}$.[61] [c] Using 0.15 μM $PHD2_{181–426}$, 10.0 μM 2OG and 5.0 μM HIF-1α $CODD_{556–574}$.[61] [d] Using 0.05 μM His_6-$AspH_{315–758}$, 3.0 μM 2OG and 1.0 μM hFX-$CP_{101–119}$.[58] [e] Using 0.15 μM KDM4A, 10.0 μM 2OG and 10.0 μM $H3_{1–15}K9me3_{1–15}$.[69] [f] Using 0.15 μM JMJD5, 2.0 μM 2OG and 2.0 μM $RSP6_{128–148}$.[70] Inhibition assays were performed using SPE-MS as described in the ESI.

FIH inhibitors reduce lipid accumulation in 3T3-L1-derived adipocytes. Genetic knockout of FIH is reported to stimulate a shift in cellular metabolism that, unusually, causes an increase in both glycolysis and oxidative metabolism, leading to increased energy consumption.[48] To inform on the proposed role of FIH in metabolic regulation, we investigated the effects of **42**, **42b** and DM-**NOFD** on lipid accumulation in 3T3-L1-derived adipocytes. Following treatment with **42** and **42b**, a dose-dependent decrease in cellular triglyceride (TG) levels was observed, as determined using a triglyceride colorimetric assay (Fig. 5F). By contrast, DM-**NOFD** had no effect on TG levels at 100 μM. At 50 μM, **42** and **42b** caused a ∼30% and ∼20% reduction in cellular TG levels, respectively, which was comparable to the effect of treatment with 20 μM obeticholic acid (25% reduction; OCA), a farnesoid X receptor (FXR) agonist that is used to treat metabolic-related conditions including primary biliary cirrhosis and non-alcoholic fatty liver disease.[94] The effect of **42** and **42b** on lipid accumulation could also be observed using Oil Red O staining (Fig. 5G). Neither **42** and **42b** exhibited apparent cytotoxicity at the concentrations used (Fig. 5H). Although further investigation is necessary, our observations are consistent with the involvement of FIH in the regulation of cellular metabolism.

Conclusions

The physiological roles of FIH are incompletely understood, including how its substrate and, potentially, its 2-oxo acid cosubstrate[60] promiscuity relate to its role in hypoxia sensing. Potent and selective small-molecule FIH inhibitors will be useful for *in vivo* functional assignment studies. Reported studies on the cellular roles of FIH have employed a prodrug diester form of the small-molecule **NOFD**,[17,29] which is a derivative of the broad-spectrum 2OG oxygenase inhibitor **NOG**. However, we have previously shown that **NOFD** inhibits other 2OG oxygenases than FIH, including AspH,[58] albeit substantially less efficiently. Nonetheless, this observation indicates that **NOFD** may not be perfectly selective for FIH inhibition considering that ∼60–70 2OG oxygenases are present in humans.[96] Thus, we were interested in identifying alternative scaffolds suitable for optimisation as *in vivo* active FIH inhibitors.

We investigated reported PHD inhibitors for FIH inhibition on the basis that PHD inhibitors such as daprodustat are reported to inhibit both PHDs and FIH,[56] to identify novel lead structures for the development of potent and selective FIH inhibitors (ESI Table S1†). Interestingly, we observed that the reported *N*-hydroxythiazole-based PHD inhibitor **BNS**[33] inhibits other 2OG oxygenases than the PHDs, including FIH, and can thus be considered as a relatively broad-spectrum 2OG oxygenase inhibitor (Table 1, entry iii). This observation suggests that previous cellular studies performed with **BNS**(-derivatives) should be interpreted with care,[17,80] including with respect to potential toxicity.

N-Hydroxythiazoles are chemically interesting metalloenzyme inhibitors because of the heavily functionalised and polar nature of the core heterocycle. Thus, **BNS** was an attractive lead structure for the development of selective FIH inhibitors, *inter alia* because its scaffold can be modified at multiple positions. Rigidification of the **BNS** structure and replacement of its sulfone and naphthalene groups afforded *N*-hydroxythiazoles that display potent FIH inhibition (IC_{50} < 0.3 μM) and a substantially improved selectivity for FIH inhibition over PHD2 compared with **BNS** (∼25-fold for **42** *vs.* ∼0.4-fold for **BNS**). High levels of selectivity were also achieved over JMJD5 (∼25-fold), KDM4A (>300-fold) and AspH (∼100-fold), the latter being of interest as AspH catalyses, like FIH, the β-hydroxylation of asparaginyl residues.[71,72]

Importantly, MS studies with isolated recombinant human 2OG oxygenases reveal that the *N*-hydroxythiazole-based FIH inhibitors show a different selectivity profile for inhibiting 2OG oxygenases than does **NOFD** (Table 6),[77] an observation that reflects the differences in their FIH binding modes, as observed in co-crystal structures with FIH (Fig. 2 and 4). Analysis of the FIH:Zn:**26** complex structure suggests that the FIH inhibition selectivity of **26**, and by implication **42**, is as a result, at least in

part, of interactions formed between **26** and residues involved in FIH substrate recognition, *i.e.* Gln203 and Tyr296. By contrast, **NOFD** achieves selectivity for FIH through its benzyl side chain, which occupies a hydrophobic pocket formed by FIH residues Tyr102, Tyr145, Gln147 and Leu186 (ESI Fig. S11†).[29] This observation implies there are, at least, two complementary strategies that can be employed to achieve selectivity for FIH inhibition over other 2OG oxygenases.

The *N*-hydroxythiazole-based FIH inhibitors have potential to help identify the physiologically relevant phenotypes of FIH inhibition, together with other inhibitors such as DM-**NOFD**. We showed that the FIH inhibitors **38**, **39** and **42**, and the ethyl ester prodrug form of **42** (*i.e.* **42b**) induce a dose-dependent increase in *EGLN3* expression, a reported FIH-dependent HIF target gene,[17,56] which was comparable to that induced by DM-**NOFD**, the dimethyl ester prodrug of **NOFD** (Fig. 5A and B). It also appeared that both **42** and **42b** reduced lipid accumulation in 3T3-L1 derived adipocytes (Fig. 5F and G), an observation which is consistent with the proposed function of FIH as a regulator of cellular metabolism.[48] The combined results thus indicate that the *N*-hydroxythiazole-based FIH inhibitors have potential for enabling cell-based and *in vivo* studies directed at investigating the potential therapeutic benefit of FIH inhibition. However, given the complexity of HIF and FIH biochemistry in cells, it cannot be ruled out that other mechanisms contribute to the biologically observed effects.

Crystallographic analyses in combination with docking studies guided compound design and will be valuable for future FIH inhibitor development programs. The FIH:Zn:*N*-hydroxythiazole complex structures indicate that the *N*-hydroxythiazole-based inhibitors bind at the FIH active site *via* competitive displacement of 2OG and its HIF-α substrate. The limited inhibitory activity of truncated *N*-hydroxythiazole derivative **14** suggests that the formation of productive interactions with the HIF-1α substrate binding site, for example with the side chains of Gln203 and Trp296, as observed in the FIH:Zn:**26** structure, is important for efficient FIH inhibition (Fig. 4B). Efficient binding to residues that engage the HIF-1α substrate may be responsible for the increased FIH potency of *N*-hydroxythiazoles compared with other PHD inhibitors, such as daprodustat, that appear to bind FIH in a similar manner.[56]

Given the modular structure and broad-spectrum 2OG oxygenase inhibitory activity of **BNS**, it is likely that the *N*-hydroxythiazole scaffold can be modified to generate selective inhibitors of other 2OG oxygenases including PHD2, JMJD5 or, at least some, JmjC KDMs. The latter is of interest because of potential roles for JmjC KDMs in the hypoxic response.[97] Note that the addition of substituents to the broad-spectrum 2OG oxygenase inhibitors **NOG** and **2,4-PDCA** has resulted in development of inhibitors of FIH[29] and JMJD5,[98] respectively, which display an improved selectivity profile with respect to the parent compounds.

The FIH:Zn:*N*-hydroxythiazole complex structures also showed that *N*-hydroxythiazoles can bind to the active site metal of FIH in a bidentate manner through the exocyclic nitrogen atom and nucleophilic hydroxyl group of the *N*-hydroxythiazole unit. Although previous studies have demonstrated the promising biological activity of *N*-hydroxythiazole-derived compounds, in addition to PHD2 inhibition,[33] for example antibacterial properties[99] and inhibition of metallo-β-lactamases (MBLs),[81] their ability to bind metals in this manner had not yet been observed in crystallographic studies. It is likely that this metal coordination motif may be useful in the development of inhibitors for other metal-containing enzymes, including for 2OG oxygenases and beyond.

Abbreviations

FIH	Factor inhibiting hypoxia-inducible factor-α
HIF	Hypoxia-inducible factor
2OG	2-Oxoglutarate
PHD	Prolyl hydroxylase domain-containing protein
AspH	Aspartate/asparagine-β-hydroxylase
KDM	N^{ϵ}-Lysine demethylase
C-TAD	C-Terminal activation domain
NOG	*N*-Oxalylglycine
EPO	Erythropoietin
PDCA	Pyridine-2,4-dicarboxylic acid
(DM)-**NOFD**	(Dimethyl) *N*-oxalyl-D-phenylalanine

Data availability

The crystal structure data for the FIH:Zn:**BNS**, FIH:Zn:**20** and FIH:Zn:**26** complex structures have been deposited in the protein data bank under PDB accession codes: 8K71 (FIH:Zn:**BNS**), 8K72 (FIH:Zn:**20**), and 8K73 (FIH:Zn:**26**).

Author contributions

T. P. C., and R. Z. R. T. synthesised the inhibitors, with assistance from J. H. M. T. P. C. carried out modelling studies/analysis of crystal structures. T. P. C., A. T., and L. B. performed the SPE-MS assays; T. P. C., R. Z. R. T., and W. F. performed the FIH:*N*-hydroxythiazole co-crystallizations. Y. N. solved and refined the FIH:*N*-hydroxythiazole complex structures. E. S, L. B., G. F., and A. B. produced and purified recombinant proteins. Y. W. performed the cell-based experiments. L. B., X. Z., and C. J. S. supervised the research. T. P. C. (original draft), L. B., and C. J. S. wrote the manuscript.

Conflicts of interest

The authors declare no competing interests.

Acknowledgements

We thank Dr Michael A. McDonough and Dr Rashed Chowdhury for initial studies on crystallography of *N*-hydroxythiazole complexes. This research was funded in part by the Wellcome Trust (106244/Z/14/Z). We thank Cancer Research UK (C8717/A18245) and the Biotechnology and Biological Sciences Research Council (BB/J003018/1 and BB/R000344/1) for funding. T. P. C. thanks the Centre for Doctoral Training in Synthesis for

Biology and Medicine for a studentship, generously supported by GlaxoSmithKline, MSD, Syngenta, and Vertex. T. P. C. thanks the Royal Commission for the Exhibition 1851 for an industrial fellowship. X. Z. thanks the National Natural Science Foundation of China (grants 81973173, 82273769, and 82322062) and the Jiangsu Provincial Funds for Distinguished Young Scientists (grant BK20211527) for funding. We thank the Diamond Light Source and staff for allocation of beam time and support. We thank the MS and NMR facilities from the Chemistry Research Laboratory, University of Oxford, for excellent support.

References

1 W. G. Kaelin Jr. and P. J. Ratcliffe, Oxygen sensing by metazoans: the central role of the HIF hydroxylase pathway, *Mol. Cell*, 2008, **30**, 393–402.
2 J. López-Barneo, R. Pardal and P. Ortega-Sáenz, Cellular mechanism of oxygen sensing, *Annu. Rev. Physiol.*, 2001, **63**, 259–287.
3 R. H. Wenger, Mammalian oxygen sensing, signalling and gene regulation, *J. Exp. Biol.*, 2000, **203**, 1253–1263.
4 R. K. Bruick, Oxygen sensing in the hypoxic response pathway: regulation of the hypoxia-inducible transcription factor, *Genes Dev.*, 2003, **17**, 2614–2623.
5 M. Safran and W. G. Kaelin Jr., HIF hydroxylation and the mammalian oxygen-sensing pathway, *J. Clin. Invest.*, 2003, **111**, 779–783.
6 C. J. Schofield and P. J. Ratcliffe, Oxygen sensing by HIF hydroxylases, *Nat. Rev. Mol. Cell Biol.*, 2004, **5**, 343–354.
7 M. Nangaku and K.-U. Eckardt, Hypoxia and the HIF system in kidney disease, *J. Mol. Med.*, 2007, **85**, 1325–1330.
8 O. Martínez-Sáez, P. G. Borau, T. Alonso-Gordoa, J. Molina-Cerrillo and E. Grande, Targeting HIF-2 α in clear cell renal cell carcinoma: a promising therapeutic strategy, *Crit. Rev. Oncol. Hematol.*, 2017, **111**, 117–123.
9 A. C. R. Epstein, J. M. Gleadle, L. A. McNeill, K. S. Hewitson, J. O'Rourke, D. R. Mole, M. Mukherji, E. Metzen, M. I. Wilson, A. Dhanda, Y.-M. Tian, N. Masson, D. L. Hamilton, P. Jaakkola, R. Barstead, J. Hodgkin, P. H. Maxwell, C. W. Pugh, C. J. Schofield and P. J. Ratcliffe, *C. elegans* EGL-9 and mammalian homologs define a family of dioxygenases that regulate HIF by prolyl hydroxylation, *Cell*, 2001, **107**, 43–54.
10 W.-C. Hon, M. I. Wilson, K. Harlos, T. D. W. Claridge, C. J. Schofield, C. W. Pugh, P. H. Maxwell, P. J. Ratcliffe, D. I. Stuart and E. Y. Jones, Structural basis for the recognition of hydroxyproline in HIF-1α by pVHL, *Nature*, 2002, **417**, 975–978.
11 J.-H. Min, H. Yang, M. Ivan, F. Gertler, W. G. Kaelin Jr. and N. P. Pavletich, Structure of an HIF-1α-pVHL complex: hydroxyproline recognition in signaling, *Science*, 2002, **296**, 1886–1889.
12 K. Tanimoto, Y. Makino, T. Pereira and L. Poellinger, Mechanism of regulation of the hypoxia-inducible factor-1α by the von Hippel-Lindau tumor suppressor protein, *EMBO J.*, 2000, **19**, 4298–4309.
13 A. A. Joharapurkar, V. B. Pandya, V. J. Patel, R. C. Desai and M. R. Jain, Prolyl hydroxylase inhibitors: a breakthrough in the therapy of anemia associated with chronic diseases, *J. Med. Chem.*, 2018, **61**, 6964–6982.
14 K. S. Hewitson, L. A. McNeill, M. V. Riordan, Y.-M. Tian, A. N. Bullock, R. W. Welford, J. M. Elkins, N. J. Oldham, S. Bhattacharya, J. M. Gleadle, P. J. Ratcliffe, C. W. Pugh and C. J. Schofield, Hypoxia-inducible factor (HIF) asparagine hydroxylase is identical to factor inhibiting HIF (FIH) and is related to the cupin structural family, *J. Biol. Chem.*, 2002, **277**, 26351–26355.
15 D. Lando, D. J. Peet, J. J. Gorman, D. A. Whelan, M. L. Whitelaw and R. K. Bruick, FIH-1 is an asparaginyl hydroxylase enzyme that regulates the transcriptional activity of hypoxia-inducible factor, *Genes Dev.*, 2002, **16**, 1466–1471.
16 P. C. Mahon, K. Hirota and G. L. Semenza, FIH-1: a novel protein that interacts with HIF-1α and VHL to mediate repression of HIF-1 transcriptional activity, *Genes Dev.*, 2001, **15**, 2675–2686.
17 M. C. Chan, N. E. Ilott, J. Schödel, D. Sims, A. Tumber, K. Lippl, D. R. Mole, C. W. Pugh, P. J. Ratcliffe, C. P. Ponting and C. J. Schofield, Tuning the transcriptional response to hypoxia by inhibiting hypoxia-inducible factor (HIF) prolyl and asparaginyl hydroxylases, *J. Biol. Chem.*, 2016, **291**, 20661–20673.
18 M. Hirsilä, P. Koivunen, V. Günzler, K. I. Kivirikko and J. Myllyharju, Characterization of the human prolyl 4-hydroxylases that modify the hypoxia-inducible factor, *J. Biol. Chem.*, 2003, **278**, 30772–30780.
19 P. Koivunen, M. Hirsilä, V. Günzler, K. I. Kivirikko and J. Myllyharju, Catalytic properties of the asparaginyl hydroxylase (FIH) in the oxygen sensing pathway are distinct from those of its prolyl 4-hydroxylases, *J. Biol. Chem.*, 2004, **279**, 9899–9904.
20 F. Dayan, D. Roux, M. C. Brahimi-Horn, J. Pouyssegur and N. M. Mazure, The oxygen sensor factor-inhibiting hypoxia-inducible factor-1 controls expression of distinct genes through the bifunctional transcriptional character of hypoxia-inducible factor-1α, *Cancer Res.*, 2006, **66**, 3688–3698.
21 H. Tarhonskaya, R. Chowdhury, I. K. H. Leung, N. D. Loik, J. S. O. McCullagh, T. D. W. Claridge, C. J. Schofield and E. Flashman, Investigating the contribution of the active site environment to the slow reaction of hypoxia-inducible factor prolyl hydroxylase domain 2 with oxygen, *Biochem. J.*, 2014, **463**, 363–372.
22 E. Flashman, L. M. Hoffart, R. B. Hamed, J. M. Bollinger Jr., C. Krebs and C. J. Schofield, Evidence for the slow reaction of hypoxia-inducible factor prolyl hydroxylase 2 with oxygen, *FEBS J.*, 2010, **277**, 4089–4099.
23 G. L. Wang and G. L. Semenza, Molecular basis of hypoxia-induced erythropoietin expression, *Curr. Opin. Hematol.*, 1996, **3**, 156–162.
24 Y. Liu, S. R. Cox, T. Morita and S. Kourembanas, Hypoxia regulates vascular endothelial growth factor gene

expression in endothelial cells: identification of a 5' enhancer, *Circ. Res.*, 1995, **77**, 638–643.

25 H. Tarhonskaya, A. P. Hardy, E. A. Howe, N. D. Loik, H. B. Kramer, J. S. O. McCullagh, C. J. Schofield and E. Flashman, Kinetic investigations of the role of factor inhibiting hypoxia-inducible factor (FIH) as an oxygen sensor, *J. Biol. Chem.*, 2015, **290**, 19726–19742.

26 E. Berra, E. Benizri, A. Ginouvès, V. Volmat, D. Roux and J. Pouysségur, HIF prolyl-hydroxylase 2 is the key oxygen sensor setting low steady-state levels of HIF-1α in normoxia, *EMBO J.*, 2003, **22**, 4082–4090.

27 A. Conejo-Garcia, M. A. McDonough, C. Loenarz, L. A. McNeill, K. S. Hewitson, W. Ge, B. M. Liénard, C. J. Schofield and I. J. Clifton, Structural basis for binding of cyclic 2-oxoglutarate analogues to factor-inhibiting hypoxia-inducible factor, *Bioorg. Med. Chem. Lett.*, 2010, **20**, 6125–6128.

28 J. M. Elkins, K. S. Hewitson, L. A. McNeill, J. F. Seibel, I. Schlemminger, C. W. Pugh, P. J. Ratcliffe and C. J. Schofield, Structure of factor-inhibiting hypoxia-inducible factor (HIF) reveals mechanism of oxidative modification of HIF-1α, *J. Biol. Chem.*, 2003, **278**, 1802–1806.

29 M. A. McDonough, L. A. McNeill, M. Tilliet, C. A. Papamicaël, Q.-Y. Chen, B. Banerji, K. S. Hewitson and C. J. Schofield, Selective inhibition of factor inhibiting hypoxia-inducible factor, *J. Am. Chem. Soc.*, 2005, **127**, 7680–7681.

30 P. E. Pergola, B. S. Spinowitz, C. S. Hartman, B. J. Maroni and V. H. Haase, Vadadustat, a novel oral HIF stabilizer, provides effective anemia treatment in nondialysis-dependent chronic kidney disease, *Kidney Int.*, 2016, **90**, 1115–1122.

31 H. Beck, M. Jeske, K. Thede, F. Stoll, I. Flamme, M. Akbaba, J.-K. Ergüden, G. Karig, J. Keldenich, F. Oehme, H.-C. Militzer, I. V. Hartung and U. Thuss, Discovery of molidustat (BAY 85-3934): a small-molecule oral HIF-prolyl hydroxylase (HIF-PH) inhibitor for the treatment of renal anemia, *ChemMedChem*, 2018, **13**, 988–1003.

32 R. A. Brigandi, B. Johnson, C. Oei, M. Westerman, G. Olbina, J. de Zoysa, S. D. Roger, M. Sahay, N. Cross, L. McMahon, V. Guptha, E. A. Smolyarchuk, N. Singh, S. F. Russ, S. Kumar, A. V. Borsukov, V. V. Marasaev, G. Prasad, G. Y. Timokhovskaya, E. V. Kolmakova, V. A. Dobronravov, E. V. Zakharova, G. Abraham, D. Packham, D. A. Zateyshchikov, G. P. Arutyunov, G. V. Volgina, K. S. Lipatov, D. V. Perlin, B. Cooper, T. Kumar Saha, O. A. Zagrebelnaya, K. S. Mehta, N. A. Koziolova, R. Fassett, N. P. Alexeeva and L. V. Lysenko, A novel hypoxia-inducible factor– prolyl hydroxylase inhibitor (GSK1278863) for anemia in CKD: a 28-day, phase 2A randomized trial, *Am. J. Kidney Dis.*, 2016, **67**, 861–871.

33 C. M. Tegley, V. N. Viswanadhan, K. Biswas, M. J. Frohn, T. A. N. Peterkin, C. Chang, R. W. Bürli, J. H. Dao, H. Veith, N. Rogers, S. C. Yoder, G. Biddlecome, P. Tagari, J. R. Allen and R. W. Hungate, Discovery of novel hydroxythiazoles as HIF-α prolyl hydroxylase inhibitors: SAR, synthesis, and modeling evaluation, *Bioorg. Med. Chem. Lett.*, 2008, **18**, 3925–3928.

34 V. L. Dengler, M. D. Galbraith and J. M. Espinosa, Transcriptional regulation by hypoxia inducible factors, *Crit. Rev. Biochem. Mol. Biol.*, 2014, **49**, 1.

35 A. Ortiz-Barahona, D. Villar, N. Pescador, J. Amigo and L. del Peso, Genome-wide identification of hypoxia-inducible factor binding sites and target genes by a probabilistic model integrating transcription-profiling data and *in silico* binding site prediction, *Nucleic Acids Res.*, 2010, **38**, 2332–2345.

36 P. Carmeliet, VEGF as a key mediator of angiogenesis in cancer, *Oncology*, 2005, **69**, 4–10.

37 G. Dobrynin, T. E. McAllister, K. B. Leszczynska, S. Ramachandran, A. J. Krieg, A. Kawamura and E. M. Hammond, KDM4A regulates HIF-1 levels through H3K9me3, *Sci. Rep.*, 2017, **7**, 11094.

38 M. E. Cockman, K. Lippl, Y.-M. Tian, H. B. Pegg, W. D. Figg Jr., M. I. Abboud, R. Heilig, R. Fischer, J. Myllyharju, C. J. Schofield and P. J. Ratcliffe, Lack of activity of recombinant HIF prolyl hydroxylases (PHDs) on reported non-HIF substrates, *Elife*, 2019, **8**, e46490.

39 M. E. Cockman, D. E. Lancaster, I. P. Stolze, K. S. Hewitson, M. A. McDonough, M. L. Coleman, C. H. Coles, X. Yu, R. T. Hay, S. C. Ley, C. W. Pugh, N. J. Oldham, N. Masson, C. J. Schofield and P. J. Ratcliffe, Posttranslational hydroxylation of ankyrin repeats in IκB proteins by the hypoxia-inducible factor (HIF) asparaginyl hydroxylase, factor inhibiting HIF (FIH), *Proc. Natl. Acad. Sci. U.S.A.*, 2006, **103**, 14767–14772.

40 M. E. Cockman, J. D. Webb and P. J. Ratcliffe, FIH-dependent asparaginyl hydroxylation of ankyrin repeat domain-containing proteins, *Ann. N. Y. Acad. Sci.*, 2009, **1177**, 9–18.

41 K. Janke, U. Brockmeier, K. Kuhlmann, M. Eisenacher, J. Nolde, H. E. Meyer, H. Mairbäurl and E. Metzen, Factor inhibiting HIF-1 (FIH-1) modulates protein interactions of apoptosis-stimulating p53 binding protein 2 (ASPP2), *J. Cell Sci.*, 2013, **126**, 2629–2640.

42 T. M. Leissing, A. P. Hardy, H. Chan, Y. Wang, A. Tumber, R. Chowdhury, T. Feng, M. L. Coleman, M. E. Cockman, H. B. Kramer, G. Berridge, R. Fischer, B. M. Kessler, P. J. Ratcliffe, X. Lu and C. J. Schofield, Factor inhibiting HIF can catalyze two asparaginyl hydroxylations in VNVN motifs of ankyrin fold proteins, *J. Biol. Chem.*, 2022, **298**, 102020.

43 M. L. Coleman, M. A. McDonough, K. S. Hewitson, C. Coles, J. Mecinovicí, M. Edelmann, K. M. Cook, M. E. Cockman, D. E. Lancaster, B. M. Kessler, N. J. Oldham, P. J. Ratcliffe and C. J. Schofield, Asparaginyl hydroxylation of the Notch ankyrin repeat domain by factor inhibiting hypoxia-inducible factor, *J. Biol. Chem.*, 2007, **282**, 24027–24038.

44 M. Yang, R. Chowdhury, W. Ge, R. B. Hamed, M. A. McDonough, T. D. W. Claridge, B. M. Kessler, M. E. Cockman, P. J. Ratcliffe and C. J. Schofield, Factor-inhibiting hypoxia-inducible factor (FIH) catalyses the post-translational hydroxylation of histidinyl residues within ankyrin repeat domains, *FEBS J.*, 2011, **278**, 1086–1097.

45 J. Kang, Y.-S. Chun, J. Huh and J.-W. Park, FIH permits NAA10 to catalyze the oxygen-dependent lysyl-acetylation of HIF-1α, *Redox Biol.*, 2018, **19**, 364–374.
46 M. Mantri, Z. Zhang, M. A. McDonough and C. J. Schofield, Autocatalysed oxidative modifications to 2-oxoglutarate dependent oxygenases, *FEBS J.*, 2012, **279**, 1563–1575.
47 M. Yang, W. Ge, R. Chowdhury, T. D. W. Claridge, H. B. Kramer, B. Schmierer, M. A. McDonough, L. Gong, B. M. Kessler, P. J. Ratcliffe, M. L. Coleman and C. J. Schofield, Asparagine and aspartate hydroxylation of the cytoskeletal ankyrin family is catalyzed by factor-inhibiting hypoxia-inducible factor, *J. Biol. Chem.*, 2011, **286**, 7648–7660.
48 J. Sim, A. S. Cowburn, A. Palazon, B. Madhu, P. A. Tyrakis, D. Macías, D. M. Bargiela, S. Pietsch, M. Gralla, C. E. Evans, T. Kittipassorn, Y. C. J. Chey, C. M. Branco, H. Rundqvist, D. J. Peet and R. S. Johnson, The factor inhibiting HIF asparaginyl hydroxylase regulates oxidative metabolism and accelerates metabolic adaptation to hypoxia, *Cell Metab.*, 2018, **27**, 898–913.
49 N. Masson, R. S. Singleton, R. Sekirnik, D. C. Trudgian, L. J. Ambrose, M. X. Miranda, Y.-M. Tian, B. M. Kessler, C. J. Schofield and P. J. Ratcliffe, The FIH hydroxylase is a cellular peroxide sensor that modulates HIF transcriptional activity, *EMBO Rep.*, 2012, **13**, 251–257.
50 Y. L. Volkova, C. Pickel, A. E. Jucht, R. H. Wenger and C. C. Scholz, The asparagine hydroxylase FIH: a unique oxygen sensor, *Antioxid. Redox Signaling*, 2022, **37**, 913–935.
51 P. H. Maxwell and K.-U. Eckardt, HIF prolyl hydroxylase inhibitors for the treatment of renal anaemia and beyond, *Nat. Rev. Nephrol.*, 2016, **12**, 157–168.
52 K. Wu, K. Zhou, Y. Wang, Y. Zhou, N. Tian, Y. Wu, D. Chen, D. Zhang, X. Wang, H. Xu and X. Zhang, Stabilization of HIF-1α by FG-4592 promotes functional recovery and neural protection in experimental spinal cord injury, *Brain Res.*, 2016, **1632**, 19–26.
53 Y. Wu, Z. Li, M. A. McDonough, C. J. Schofield and X. Zhang, Inhibition of the oxygen-sensing asparaginyl hydroxylase factor inhibiting hypoxia-inducible factor: a potential hypoxia response modulating strategy, *J. Med. Chem.*, 2021, **64**, 7189–7209.
54 L. Brewitz, A. Tumber, A. Thalhammer, E. Salah, K. E. Christensen and C. J. Schofield, Synthesis of novel pyridine-carboxylates as small-molecule inhibitors of human Aspartate/asparagine-β-hydroxylase, *ChemMedChem*, 2020, **15**, 1139–1149.
55 M. C. Chan, O. Atasoylu, E. Hodson, A. Tumber, I. K. H. Leung, R. Chowdhury, V. Gómez-Pérez, M. Demetriades, A. M. Rydzik, J. Holt-Martyn, Y.-M. Tian, T. Bishop, T. D. W. Claridge, A. Kawamura, C. W. Pugh, P. J. Ratcliffe and C. J. Schofield, Potent and selective triazole-based inhibitors of the hypoxia-inducible factor prolyl-hydroxylases with activity in the murine brain, *PLoS One*, 2015, **10**, e0132004.
56 T.-L. Yeh, T. M. Leissing, M. I. Abboud, C. C. Thinnes, O. Atasoylu, J. P. Holt-Martyn, D. Zhang, A. Tumber, K. Lippl, C. T. Lohans, I. K. H. Leung, H. Morcrette, I. J. Clifton, T. D. W. Claridge, A. Kawamura, E. Flashman, X. Lu, P. J. Ratcliffe, R. Chowdhury, C. W. Pugh and C. J. Schofield, Molecular and cellular mechanisms of HIF prolyl hydroxylase inhibitors in clinical trials, *Chem. Sci.*, 2017, **8**, 7651–7668.
57 C. J. Brereton, L. Yao, E. R. Davies, Y. Zhou, M. Vukmirovic, J. A. Bell, S. Wang, R. A. Ridley, L. S. N. Dean, O. G. Andriotis, F. Conforti, L. Brewitz, S. Mohammed, T. Wallis, A. Tavassoli, R. M. Ewing, A. Alzetani, B. G. Marshall, S. V. Fletcher, P. J. Thurner, A. Fabre, N. Kaminski, L. Richeldi, A. Bhaskar, C. J. Schofield, M. Loxham, D. E. Davies, Y. Wang and M. G. Jones, Pseudohypoxic HIF pathway activation dysregulates collagen structure-function in human lung fibrosis, *Elife*, 2022, **11**, e69348.
58 L. Brewitz, A. Tumber, I. Pfeffer, M. A. McDonough and C. J. Schofield, Aspartate/asparagine-β-hydroxylase: a high-throughput mass spectrometric assay for discovery of small molecule inhibitors, *Sci. Rep.*, 2020, **10**, 8650.
59 N. R. Rose, E. C. Y. Woon, G. L. Kingham, O. N. F. King, J. Mecinović, I. J. Clifton, S. S. Ng, J. Talib-Hardy, U. Oppermann, M. A. McDonough and C. J. Schofield, Selective inhibitors of the JMJD2 histone demethylases: combined nondenaturing mass spectrometric screening and crystallographic approaches, *J. Med. Chem.*, 2010, **53**, 1810–1818.
60 Y. Nakashima, L. Brewitz, A. Tumber, E. Salah and C. J. Schofield, 2-Oxoglutarate derivatives can selectively enhance or inhibit the activity of human oxygenases, *Nat. Commun.*, 2021, **12**, 6478.
61 J. P. Holt-Martyn, R. Chowdhury, A. Tumber, T.-L. Yeh, M. I. Abboud, K. Lippl, C. T. Lohans, G. W. Langley, W. Figg Jr., M. A. McDonough, C. W. Pugh, P. J. Ratcliffe and C. J. Schofield, Structure-activity relationship and crystallographic studies on 4-hydroxypyrimidine HIF prolyl hydroxylase domain inhibitors, *ChemMedChem*, 2020, **15**, 270–273.
62 N. R. Rose, M. A. McDonough, O. N. F. King, A. Kawamura and C. J. Schofield, Inhibition of 2-oxoglutarate dependent oxygenases, *Chem. Soc. Rev.*, 2011, **40**, 4364–4397.
63 R. I. Dowell and E. M. Hadley, Novel inhibitors of prolyl 4-hydroxylase, *J. Med. Chem.*, 1992, **35**, 800–804.
64 J. H. Dao, R. J. M. Kurzeja, J. M. Morachis, H. Veith, J. Lewis, V. Yu, C. M. Tegley and P. Tagari, Kinetic characterization and identification of a novel inhibitor of hypoxia-inducible factor prolyl hydroxylase 2 using a time-resolved fluorescence resonance energy transfer-based assay technology, *Anal. Biochem.*, 2009, **384**, 213–223.
65 M. Yang, A. P. Hardy, R. Chowdhury, N. D. Loik, J. S. Scotti, J. S. O. McCullagh, T. D. W. Claridge, M. A. McDonough, W. Ge and C. J. Schofield, Substrate selectivity analyses of Factor Inhibiting Hypoxia-Inducible Factor, *Angew. Chem.*, 2013, **125**, 1744–1748.
66 C. E. Dann III, R. K. Bruick and J. Deisenhofer, Structure of factor-inhibiting hypoxia-inducible factor 1: an asparaginyl hydroxylase involved in the hypoxic response pathway, *Proc. Natl. Acad. Sci. U.S.A.*, 2002, **99**, 15351–15356.

67 W. D. Figg Jr., M. A. McDonough, R. Chowdhury, Y. Nakashima, Z. Zhang, J. P. Holt-Martyn, A. Krajnc and C. J. Schofield, Structural basis of prolyl hydroxylase domain inhibition by molidustat, *ChemMedChem*, 2021, **16**, 2082–2088.

68 S. Linke, C. Stojkoski, R. J. Kewley, G. W. Booker, M. L. Whitelaw and D. J. Peet, Substrate requirements of the oxygen-sensing asparaginyl hydroxylase factor-inhibiting hypoxia-inducible factor, *J. Biol. Chem.*, 2004, **279**, 14391–14397.

69 S. E. Hutchinson, M. V. Leveridge, M. L. Heathcote, P. Francis, L. Williams, M. Gee, J. Munoz-Muriedas, B. Leavens, A. Shillings, E. Jones, P. Homes, S. Baddeley, C.-w. Chung, A. Bridges and A. Argyrou, Enabling lead discovery for histone lysine demethylases by high-throughput RapidFire mass spectrometry, *J. Biomol. Screening*, 2012, **17**, 39–48.

70 A. Tumber, E. Saleh, L. Brewitz, T. P. Corner and C. J. Schofield, Kinetic and inhibition studies on human Jumonji-C (JmjC) domain-containing protein 5, *RSC Chem. Biol.*, 2023, **4**, 399–413.

71 J. Stenflo, E. Holme, S. Lindstedt, N. Chandramouli, L.-H. Huang, J. P. Tam and R. B. Merrifield, Hydroxylation of aspartic acid in domains homologous to the epidermal growth factor precursor is catalyzed by a 2-oxoglutarate-dependent dioxygenase, *Proc. Natl. Acad. Sci. U.S.A.*, 1989, **86**, 444–447.

72 L. Brewitz, B. C. Onisko and C. J. Schofield, Combined proteomic and biochemical analyses redefine the consensus sequence requirement for epidermal growth factor-like domain hydroxylation, *J. Biol. Chem.*, 2022, **298**, 102129.

73 H. Wang, X. Zhou, M. Wu, C. Wang, X. Zhang, Y. Tao, N. Chen and J. Zang, Structure of the JmjC-domain-containing protein JMJD5, *Acta Crystallogr. D*, 2013, **69**, 1911–1920.

74 P. A. Del Rizzo, S. Krishnan and R. C. Trievel, Crystal structure and functional analysis of JMJD5 indicate an alternate specificity and function, *Mol. Cell. Biol.*, 2012, **32**, 4044–4052.

75 Z. Chen, J. Zang, J. Whetstine, X. Hong, F. Davrazou, T. G. Kutateladze, M. Simpson, Q. Mao, C.-H. Pan, S. Dai, J. Hagman, K. Hansen, Y. Shi and G. Zhang, Structural insights into histone demethylation by JMJD2 family members, *Cell*, 2006, **125**, 691–702.

76 L. J. Walport, R. J. Hopkinson, R. Chowdhury, Y. Zhang, J. Bonnici, R. Schiller, A. Kawamura and C. J. Schofield, Mechanistic and structural studies of KDM-catalysed demethylation of histone 1 isotype 4 at lysine 26, *FEBS Lett.*, 2018, **592**, 3264–3273.

77 R. Chowdhury, J. I. Candela-Lena, M. C. Chan, D. J. Greenald, K. K. Yeoh, Y.-M. Tian, M. A. McDonough, A. Tumber, N. R. Rose, A. Conejo-Garcia, M. Demetriades, S. Mathavan, A. Kawamura, M. K. Lee, F. van Eeden, C. W. Pugh, P. J. Ratcliffe and C. J. Schofield, Selective small molecule probes for the hypoxia inducible factor (HIF) prolyl hydroxylases, *ACS Chem. Biol.*, 2013, **8**, 1488–1496.

78 I. Pfeffer, L. Brewitz, T. Krojer, S. A. Jensen, G. T. Kochan, N. J. Kershaw, K. S. Hewitson, L. A. McNeill, H. Kramer, M. Münzel, R. J. Hopkinson, U. Oppermann, P. A. Handford, M. A. McDonough and C. J. Schofield, Aspartate/asparagine-β-hydroxylase crystal structures reveal an unexpected epidermal growth factor-like domain substrate disulfide pattern, *Nat. Commun.*, 2019, **10**, 4910.

79 R. Chowdhury, I. K. H. Leung, Y.-M. Tian, M. I. Abboud, W. Ge, C. Domene, F.-X. Cantrelle, I. Landrieu, A. P. Hardy, C. W. Pugh, P. J. Ratcliffe, T. D. W. Claridge and C. J. Schofield, Structural basis for oxygen degradation domain selectivity of the HIF prolyl hydroxylases, *Nat. Commun.*, 2016, **7**, 12673.

80 K. Thirstrup, S. Christensen, H. A. Møller, A. Ritzén, A.-L. Bergström, T. N. Sager and H. S. Jensen, Endogenous 2-oxoglutarate levels impact potencies of competitive HIF prolyl hydroxylase inhibitors, *Pharmacol. Res.*, 2011, **64**, 268–273.

81 A. Makena, S. S. van Berkel, C. Lejeune, R. J. Owens, A. Verma, R. Salimraj, J. Spencer, J. Brem and C. J. Schofield, Chromophore-linked substrate (CLS405): probing metallo-β-lactamase activity and inhibition, *ChemMedChem*, 2013, **8**, 1923–1929.

82 H. Wissmann and H.-J. Kleiner, New peptide synthesis, *Angew. Chem., Int. Ed.*, 1980, **19**, 133–134.

83 S. B. Hatch, C. Yapp, R. C. Montenegro, P. Savitsky, V. Gamble, A. Tumber, G. F. Ruda, V. Bavetsias, O. Fedorov, B. Atrash, F. Raynaud, R. Lanigan, L. Carmichael, K. Tomlin, R. Burke, S. M. Westaway, J. A. Brown, R. K. Prinjha, E. D. Martinez, U. Oppermann, C. J. Schofield, C. Bountra, A. Kawamura, J. Blagg, P. E. Brennan, O. Rossanese and S. Müller, Assessing histone demethylase inhibitors in cells: lessons learned, *Epigenet. Chromatin*, 2017, **10**, 9.

84 G. Joberty, M. Boesche, J. A. Brown, D. Eberhard, N. S. Garton, P. G. Humphreys, T. Mathieson, M. Muelbaier, N. G. Ramsden, V. Reader, A. Rueger, R. J. Sheppard, S. M. Westaway, M. Bantscheff, K. Lee, D. M. Wilson, R. K. Prinjha and G. Drewes, Interrogating the druggability of the 2-oxoglutarate-dependent dioxygenase target class by chemical proteomics, *ACS Chem. Biol.*, 2016, **11**, 2002–2010.

85 J. Rautio, H. Kumpulainen, T. Heimbach, R. Oliyai, D. Oh, T. Järvinen and J. Savolainen, Prodrugs: design and clinical applications, *Nat. Rev. Drug Discovery*, 2008, **7**, 255–270.

86 T. Wang, R. Zhang, Y. Liu, Z. Fang, H. Zhang, Y. Fan, S. Yang and R. Xiang, Discovery of a new class of JMJD6 inhibitors and structure–activity relationship study, *Bioorg. Med. Chem. Lett.*, 2021, **44**, 128109.

87 S. M. Westaway, A. G. S. Preston, M. D. Barker, F. Brown, J. A. Brown, M. Campbell, C.-w. Chung, G. Drewes, R. Eagle, N. Garton, L. Gordon, C. Haslam, T. G. Hayhow, P. G. Humphreys, G. Joberty, R. Katso, L. Kruidenier, M. Leveridge, M. Pemberton, I. Rioja, G. A. Seal, T. Shipley, O. Singh, C. J. Suckling, J. Taylor, P. Thomas,

D. M. Wilson, K. Lee and R. K. Prinjha, Cell penetrant inhibitors of the KDM4 and KDM5 families of histone lysine demethylases. 2. Pyrido[3,4-*d*]pyrimidin-4(3*H*)-one derivatives, *J. Med. Chem.*, 2016, **59**, 1370–1387.

88 A. Aihara, C. K. Huang, M. J. Olsen, Q. Lin, W. Chung, Q. Tang, X. Dong and J. R. Wands, A cell-surface β-hydroxylase is a biomarker and therapeutic target for hepatocellular carcinoma, *Hepatol*, 2014, **60**, 1302–1313.

89 W. Zheng, X. Wang, J. Hu, B. Bai and H. Zhu, Diverse molecular functions of aspartate β-hydroxylase in cancer (Review), *Oncol. Rep.*, 2020, **44**, 2364–2372.

90 M. Kanwal, M. Smahel, M. Olsen, J. Smahelova and R. Tachezy, Aspartate β-hydroxylase as a target for cancer therapy, *J. Exp. Clin. Cancer Res.*, 2020, **39**, 163.

91 L. Lavaissiere, S. Jia, M. Nishiyama, S. de la Monte, A. M. Stern, J. R. Wands and P. A. Friedman, Overexpression of human aspartyl(asparaginyl)beta-hydroxylase in hepatocellular carcinoma and cholangiocarcinoma, *J. Clin. Invest.*, 1996, **98**, 1313–1323.

92 L. Brewitz, Y. Nakashima, A. Tumber, E. Salah and C. J. Schofield, Fluorinated derivatives of pyridine-2,4-dicarboxylate are potent inhibitors of human 2-oxoglutarate dependent oxygenases, *J. Fluorine Chem.*, 2021, **247**, 109804.

93 X. Dong, Q. Lin, A. Aihara, Y. Li, C.-K. Huang, W. Chung, Q. Tang, X. Chen, R. Carlson, C. Nadolny, G. Gabriel, M. Olsen and J. R. Wands, Aspartate β-hydroxylase expression promotes a malignant pancreatic cellular phenotype, *Oncotarget*, 2015, **6**, 1231–1248.

94 R. Pellicciari, S. Fiorucci, E. Camaioni, C. Clerici, G. Costantino, P. R. Maloney, A. Morelli, D. J. Parks and T. M. Willson, 6α-Ethyl-chenodeoxycholic acid (6-ECDCA), a potent and selective FXR agonist endowed with anticholestatic activity, *J. Med. Chem.*, 2002, **45**, 3569–3572.

95 M. Ishiyama, H. Tominaga, M. Shiga, K. Sasamoto, Y. Ohkura and K. Ueno, A combined assay of cell viability and *in vitro* cytotoxicity with a highly water-soluble tetrazolium salt, neutral red and crystal violet, *Biol. Pharm. Bull.*, 1996, **19**, 1518–1520.

96 M. S. Islam, T. M. Leissing, R. Chowdhury, R. J. Hopkinson and C. J. Schofield, 2-Oxoglutarate-dependent oxygenases, *Annu. Rev. Biochem.*, 2018, **87**, 585–620.

97 R. L. Hancock, N. Masson, K. Dunne, E. Flashman and A. Kawamura, The activity of JmjC histone lysine demethylase KDM4A is highly sensitive to oxygen concentrations, *ACS Chem. Biol.*, 2017, **12**, 1011–1019.

98 L. Brewitz, Y. Nakashima, S. K. Piasecka, E. Salah, S. C. Fletcher, A. Tumber, T. P. Corner, T. J. Kennedy, G. Fiorini, A. Thalhammer, K. E. Christensen, M. L. Coleman and C. J. Schofield, 5-Substituted pyridine-2,4-dicarboxylate derivatives Have potential for selective inhibition of human Jumonji-C Domain-Containing Protein 5, *J. Med. Chem.*, 2023, **66**, 10849–10865.

99 E. Perrone, M. Alpegiani, F. Giudici, F. Buzzetti, G. Nannini, G. Meinardi, S. Grasso, A. Bianchi and I. de Carneri, Cephalosporins. VII. Synthesis and antibacterial activity of new cephalosporins bearing a 2-imino-3-hydroxythiazoline (2-aminothiazole *N*-oxide) in the C-7 acylamino side chain, *J. Antibiot.*, 1984, **37**, 1423–1440.